DEVELOPMENT OF HYDROGELS VIA PHOTOCROSSLINKING OF WOOL PROTEINS

A Thesis Submitted to
the Graduate School of Engineering and Sciences of
İzmir Institute of Technology
in Partial Fulfillments of the Requirements for the Degree of

MASTER OF SCIENCE

in Chemical Engineering

by
İrem YAKAR

July 2024

İZMİR

We approve the thesis of **İrem YAKAR**

Examining Committee Members:

Assoc. Prof. Dr. Ayben TOP
Department of Chemical Engineering, İzmir Institute of Technology

Prof. Dr. Aslı Yüksel ÖZŞEN
Department of Chemical Engineering, İzmir Institute of Technology

Assoc. Prof. Dr. Canan URAZ
Department of Chemical Engineering, Ege University

10 July 2024

Assoc. Prof. Dr. Ayben TOP
Supervisor, Department of Chemical Engineering, İzmir Institute of Technology

Prof. Dr. Aysun SOFUOĞLU
Head of the Department of Chemical Engineering

Prof. Dr. Mehtap EANES
Head of the Graduate School of Engineering and Science

ACKNOWLEDGEMENTS

I would like to express my deepest gratitude to those who have supported and guided me throughout this journey of completing my MSc thesis.

First and foremost, I am profoundly grateful to my supervisor, Assoc. Prof. Dr. Ayben TOP, for her invaluable guidance, patience, and encouragement throughout this research. Her expert advice and insightful feedback were crucial in shaping this thesis and pushing me to achieve my best. It has been a great honor and privilege to work with her.

I would also like to thank the members of my thesis committee, Prof. Dr. Aslı Yüksel ÖZŞEN, and Assoc. Prof. Dr. Canan URAZ, for their time, effort, and valuable suggestions that significantly improved the quality of my work.

Special thanks to my colleagues and friends, Burcu SIRMA TARIM, Selin ŞEN, Gamze AYDOĞAN, Damla YALÇIN GÖL, Bahriyenur ARABACI, Dr. Alperay TARIM, Simge KOSTİK, Özüm ÖZBEK, Büşra SEZEN, Yağmur ÇETİN, Onur İPEK, Bulutcem ÖCAL, Merve PERPELEK, Dr. Sedef TAMBURACI, Ecem ONUK, and Simel EDİZ, İdil SAVRU for their constant support, stimulating discussions, and for making this journey a memorable one. Their camaraderie were a source of strength for me.

I am deeply appreciative of the administrative and technical support provided by Dr. Özlem ÇAĞLAR DUVARCI, Yekta GÜNAY, Evrim PAŞIK, Belgin TUNÇER KIRKAR, Dane RUSÇUKLU. Their efficiency and dedication made this study smoother and more manageable. I would also like to thank IZTECH IRC, specifically IZTECH CFB, for the use of instruments of UV-Vis Spectrophotometer, ATR-FTIR Spectroscopy, Zeta-Sizer, and antimicrobial laboratory.

I owe a debt of gratitude to my family, especially my dear mother, Gülhan ÜNLÜ, for her unwavering support, understanding, and love. Her belief in me kept me motivated and focused, even during the most challenging times.

Finally, I would like to acknowledge the financial support provided by IZTECH Research Foundation for the BAP Project with a grant number of 2023İYTE-1-0011 and the TÜBİTAK Project with a grant number of 223M522.

To everyone who contributed to this thesis in any way, I extend my heartfelt thanks.

ABSTRACT

DEVELOPMENT OF HYDROGELS VIA PHOTOCROSSLINKING OF WOOL PROTEINS

Hydrogels, with high water absorption capacity and tissue-like properties, create a moist environment ideal for wound healing. This study focuses on synthesizing bioactive gallic acid (GA) and carbon dots (CDs) containing hybrid hydrogels based on oxidized keratin (KTS), a natural protein, and Pluronic F127, a synthetic polymer for wound healing applications. Methacrylated forms of the KTS and F127 (KTSMA and F127MA) were synthesized using methacrylic anhydride, and the functionalized forms were confirmed using spectroscopic methods. KTSMA and F127MA were cross-linked under UV light using an Irgacure 2959 photoinitiator to form self-standing hydrogels. Three hydrogels were prepared: K4 (4% KTSMA), K7.5 (7.5% KTSMA), and KP7.5 (4% KTSMA + 3.5% F127MA), and their viscoelastic, swelling, degradation and morphological properties were determined. Cell proliferation tests showed that all the hydrogels supported cell growth. KP7.5 hydrogels exhibited robust mechanical and degradation properties. Carbon dots were synthesized using curcumin and l-lysine and shown to have modest antibacterial properties against *S. aureus*. Their structural and optical properties were characterized. Multifunctional hydrogels, KPGA, KPCD, and KPGACD, were obtained by incorporating GA and the CDs into the KP7.5 hydrogel. GA-containing hydrogels exhibited notable antioxidant activity, as assessed by the DPPH test. Considering their biocompatibility, these hydrogels have potential use in wound healing applications.

ÖZET

YÜN PROTEİNLERİNİN IŞIKLA ÇAPRAZ BAĞLANMASI İLE HİDROJELLERİN GELİŞTİRİLMESİ

Yüksek su emme kapasitesine ve doku benzeri özelliklere sahip hidrojeller, yara iyileşmesi için ideal nemli bir ortam sağlamaktadır. Bu çalışma, yara iyileştirme uygulamaları için doğal bir protein olan oksitlenmiş keratin (KTS) ve sentetik bir polimer olan Pluronic F127 bazlı biyoaktif gallik asit (GA) ve karbon noktaları (CD'ler) içeren hibrit hidrojellerin sentezlenmesine odaklanmıştır. KTS ve F127'nin metakrilatlanmış formları (KTSMA ve F127MA) metakrilik anhidrit kullanılarak sentezlenmiş ve fonksiyonelleştirilmiş formlar spektr oskopik yöntemler kullanılarak doğrulanmıştır. KTSMA ve F127MA, kendi kendini destekleyen hidrojeller oluşturmak için Irgacure 2959 fotobaşlatıcı kullanılarak UV ışığı altında çapraz bağlanmıştır. Üç hidrojel hazırlanmıştır: K4 (%4 KTSMA), K7.5 (%7.5 KTSMA) ve KP7.5 (%4 KTSMA + %3.5 F127MA) ve bunların viskoelastik, şişme, bozunma ve morfolojik özellikleri belirlenmiştir. Hücre proliferasyon testleri, tüm hidrojellerin hücre büyümesini desteklediğini göstermiştir. KP7.5 hidrojelleri kararlı mekanik ve bozunma özellikleri sergilemiştir. Karbon noktalar kurkumin ve l-lizin kullanılarak sentezlenmiş ve *S. aureus*'a karşı ılımlı antibakteriyel özelliklere sahip olduğu gösterilmiştir. Karbon noktaların yapısal ve optik özellikleri karakterize edilmiştir. Çok işlevli hidrojeller, KPGA, KPCD ve KPGACD, GA ve CD'lerin KP7.5 hidrojeline dahil edilmesiyle elde edilmiştir. GA içeren hidrojeller, DPPH testi ile değerlendirildiği üzere kayda değer antioksidan aktivite sergilemiştir. Biyouyumlulukları göz önüne alındığında, bu hidrojeller yara iyileştirme uygulamalarında potansiyel kullanıma sahiptir.

TABLE OF CONTENTS

LIST OF FIGURES

Figure **Page**

Figure **Page**

LIST OF TABLES

Table **Page**

CHAPTER 1

INTRODUCTION

In this chapter, the structure of skin and hydrogels used for wound healing applications were explained, and the characteristics of wound dressing hydrogels were investigated.

1.1. Skin Structure

Skin, the biggest and most vital organ in the body, is a barrier from the outside world and covers most of the physiological functions critical for the survival of mammals and humans, such as sensing, protecting, and maintaining homeostasis.[1] Its barrier function ensures the body's endurance in variable temperatures, humidity levels, and exposure to hazardous elements (e.g., radiation, chemicals, pathogens, allergens, and fungi). Homeostatic roles of the skin include blood pressure management, vitamin D synthesis initialization, and excretory functions. The skin can also detect external stimuli such as heat, pressure, discomfort, allergens, and the invasion of microorganisms, which can be associated with its sensory functions. In addition to these crucial properties, the skin can continuously repair and regenerate itself. [2]

The skin has three layers: epidermis, dermis, and hypodermis (Figure 1.1).[3] Microscopic image of epidermis and dermis is given in Figure 1.2.[4] These three layers work together to prevent water loss and protect the body from external threats.[5] The epidermis, the top layer, consists of specialized cells called keratinocytes, which produce keratin, a tough protein necessary for protection. In the middle layer, the dermis comprises the primary structural protein, collagen, which forms a network of fibers. The subcutaneous tissue, or hypodermis, is the bottom layer and includes clusters of fat cells called adipocytes. The thickness of these layers differs according to the body's anatomical location. [6]

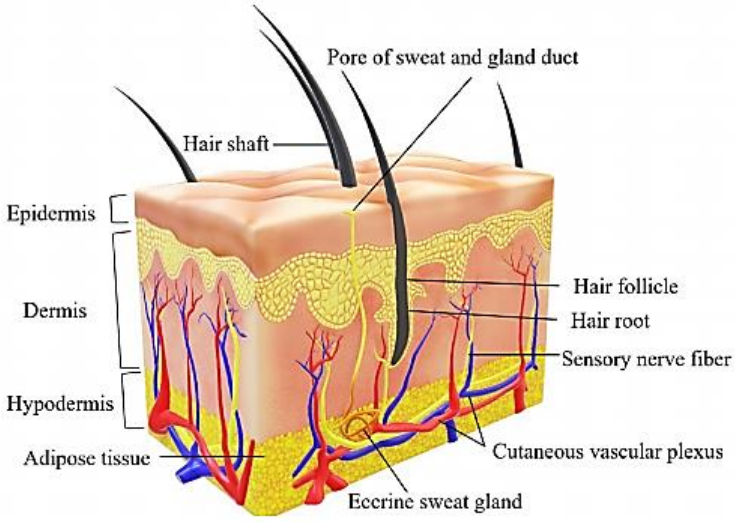

Figure 1.1. Human Skin Structure.[3]

The term "epidermis" originated from the Greek prefix "epi," i.e., outer, and the Greek word "derma," i.e., skin. The epidermis is the outermost layer of the skin, which directly interacts with the environment. A unique characteristic of the epidermis is its avascular structure, which means it lacks a vascular system or blood vessels. The main components of the epidermis are flat, layered, and keratinized epithelial tissue. The thickness of the epidermis typically consists of four to five layers of epithelial cells, and it varies depending on the region of the body.[7]

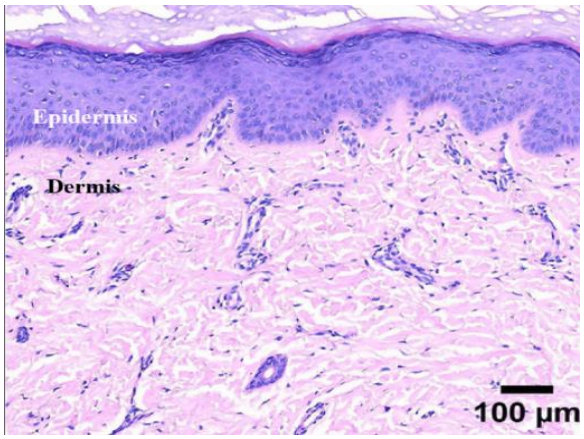

Figure 1.2. Microscopic image of Epidermis and Dermis.[4]

The dermis, middle layer, is made up of elastic and fibrous tissue, this provides structural support and nourishment. The dermis is also divided into two layers of reticular and papillary dermis (Figure 1.3).[8] These two layers are divided by the dermo-epidermal junction, characterized by loosely distributed collagen fibers. The dermis consists of various stromal cells such as fibroblasts and fibrocytes are present, along with structural components like blood and lymph vessels. Lastly, a wide variety of myeloid and lymphoid immune cells reside in or migrate through the dermis. [9]

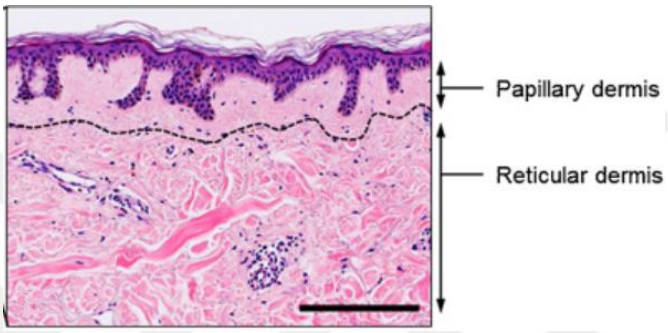

Figure 1.3. Microscopic image for the layers of dermis.[8]

The hypodermis is the deepest layer of the skin. This layer mainly comprises spherical adipocytes, fibroblasts, macrophages, blood vessels, and connective tissue composed of collagen and elastin. The primary role of the hypodermis is to support the skin's neural and circulatory systems, along with attaching the skin to the underlying muscles. Additionally, it is an energy store; it absorbs impacts and supplies heat insulation.[2]

1.2. Definition of Wound and Wound Types

Wounds can occur with damage to the epidermis layer of the skin. These damages can be surgical procedures, trauma, pathological conditions like diabetes or vascular disorders, and external forces like pressure, burns, and cuts.[10,11] It is important to restore tissue integrity and maintain homeostasis after a damage, for this reason, various intracellular and intercellular pathways must be activated and synchronized. These

pathways include inflammatory pathways, the blood coagulation cascade, and initiation of immune system cells. Different cell types undergo important changes in gene expression and phenotype, leading to cell proliferation, differentiation, and migration.[12]

The wounds are classified as either acute or chronic, depending on their underlying causes and outcomes.[10]

1.2.1. Acute Wounds and Acute Wound Healing

The pathway of wound healing following the skin injury necessitates communication among the various cellular components within the diverse compartments of the skin and its extracellular matrix (epidermis).[13]

Acute wound healing goes through four phases: hemostasis, inflammation, proliferation, and remodeling (Figure 1.4).[14] Hemostasis is, the initial response to an acute wound. It serves to halt bleeding and prevent blood loss. This phase is followed by the inflammatory phase, initiated by skin damage, it triggers a complex immune response to clear invading pathogens from the wound and prepare the tissue for structural restoration. The proliferation consists of the concurrent development of granulation tissue, neovascularization, and re-epithelialization. Lastly, for the remodeling phase, the granulation tissue gets replaced by scar tissue and immune cells are sent from the epidermis. These immune cells either migrate to the dermis or undergo apoptosis.[15]

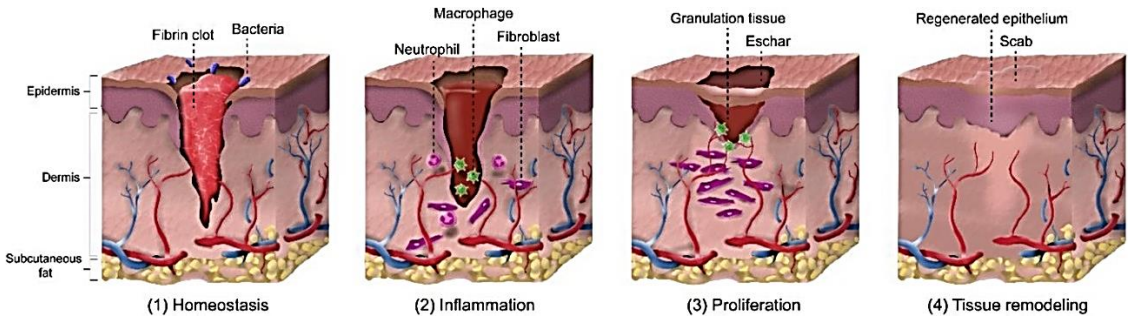

Figure 1.4. Four Stages of Wound Healing.[14]

This acute wound healing, also known as physiological wound healing, is a gradual process that results in the closure of the wound over days or weeks, depending on the size and depth of the damage to the epidermis and dermis layers of the skin.[11,16]

1.2.2. Chronic Wounds and Chronic Wound Healing

Chronic wounds are characterized as deficiencies in the skin's barrier that have not been promptly and systematically repaired to restore the skin's structural and functional integrity. The comparison of acute and chronic wound healing is given in Figure 1.5.[3] Essentially, any skin lesion has the potential to progress to a chronic wound, prompting classification based on the underlying causes. Diabetes mellitus, local pressure effects, and vascular insufficiency are non-healing skin lesions' main causes and classifications. However, systemic variables that also contribute to poor wound healing including advanced age, concurrent medical conditions, prolonged mechanical stress, and reduced nutritional or immunological state.[13]

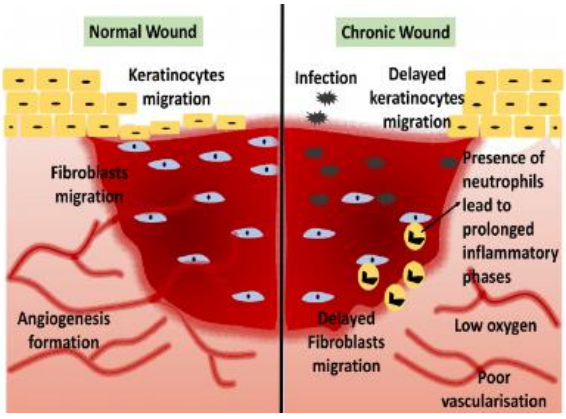

Figure 1.5. The comparison between normal and chronic wounds.[3]

During the healing process of chronic wounds, dressings have been used to directly contact the wound, protect it from further complications, and promote healing. These dressings are called wound dressings. Traditionally, dressings made of natural

fibrous materials such as non-greasy cotton gauze, gauze strips, cotton balls, and cotton fibers are used to dry, cover, and protect the wound (Figure 1.6).[17] However, these wound dressings have lower rates of wound healing because they absorb moisture from the wound to a large extent.[16] With advancements in technology and materials, new-generation wound dressings have emerged, providing an environment suitable for the wound and accelerating the healing process while overcoming the shortcomings of traditional wound dressings.[18]

Figure 1.6. Historical Timeline of Wound Dressings.[17]

1.3. Requirements of an Ideal Wound Dressing

An ideal wound dressing should possess the following characteristics: (1) it should control moisture around the wound, (2) allow significant gas transmission, (3) eliminate excess leakage, (4) protect the wound from infections and microorganisms, (5) reduce surface necrosis of the wound, (6) provide mechanical protection, (7) be easily changeable and removable, (8) be biocompatible, bioresorbable, elastic, and non-toxic, (9) alleviate wound pain, and (10) be cost-effective.[19]

1.3.1. Modern Wound Dressings

According to the requirements of the ideal wound dressings, modern wound dressings that are being used today are: (1) Hydrogel dressings, (2) Semi-permeable film dressings (3) Foam dressings, (4) Nanofiber dressings, (5) Hydrocolloid dressings, (6) Alginate dressings, and (7) Bioactive dressings given in Table 1.1.[18]

Table 1.1. Some of Modern Wound Dressings and Their Examples.

Type of Dressing	Description	Commercial Examples
Hydrogel Dressings	Hydrogels consist of about 90% water by weight and 10% natural or synthetic polymers by weight. This high water content is crucial for treating dry and necrotic wounds. The moist environment facilitated by hydrogels promotes the cellular wound healing process and enables effective debridement, which involves removing necrotic tissue and foreign material, thanks to the absorbent properties of hydrogel materials [20]	Nu-gel™ (Johnson & Johnson, Ascot, UK), Purilon™ (Coloplast)[21]
Semi-Permeable Film Dressings	Film dressings are thin, transparent sheets made of adhesive polyurethane that are resistant to liquids and bacteria, yet allow the passage of gas and water vapor. They are flexible and easily conform to wounds of different shapes and angles. This quality enables convenient wound observation without the need to remove the dressing [22]	Opsite™, Tegaderm™, Biooclusive ™ [16]

(cont. on next page)

Table 1.1 (cont.).

Foam Dressings	Foam dressings are often made up of a polyurethane or silicone core surrounded by a semi-occlusive coating. The outer layer, which varies in moisture vapor transmission rates based on the manufacturer, allows water vapor to travel through while protecting against bacterial intrusion or leakage. The polyurethane core enhances the dressing's absorbing characteristics. The cushioning properties of these dressings give the patient a great deal of comfort. They can be adherent or non-adherent, and in this case, a second film might be required. Foam dressings are very useful in exudative cavities and over bony prominences. They should be replaced as needed, usually once or twice a week, or more frequently if they get saturated with exudate. As wounds progress through healing stages, their characteristics change, and the optimal benefits of the initial dressing may be maximized, prompting a switch to a different type of dressing [23]	Lyofoam1 (Conva Tec) and Allevyn1 (Smith and Nephew) [21]
Nanofiber Dressings	About their numerous unique advantageous qualities, such as their morphological characteristics, higher surface-to-volume ratio, improved porosity, oxygen permeability, and modifiable nanopatterning, electrospun nanofibrous wound dressings are forward-looking [24]	

1.4. Hydrogels

Hydrogels are three-dimensional polymer networks with a hydrophilic nature, able to absorb substantial amounts of water and biological fluids, mimicking biological tissue when they swell. An image of a hydrogel is given in Figure 1.7. [25] Due to their similarity to natural tissue, hydrogels have garnered substantial attention in academic and research domains since its discovery in 1960 by Wichterle and Lim. [26–28]

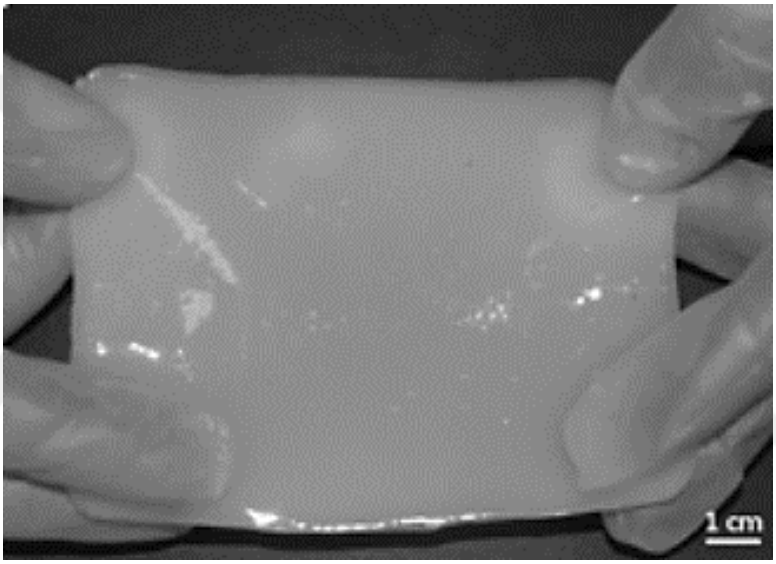

Figure 1.7. Photograph of a Hydrogel. [25]

Hydrogels can be categorized based on many properties, such as, polymer source, crosslinking, physical appearance, configuration and electric charge.[27]

1.4.1. Hydrogel Crosslinking

Crosslinking is an essential property for hydrogels to prevent the dissolution of hydrophilic polymer chains in an aqueous environment. A wide variety of methods has been employed to establish these crosslinks while preparing hydrogels.[29]

Two main types of crosslinking can be investigated as chemical and physical crosslinking. Chemically crosslinked hydrogels consist of covalent bonds between different polymer chains, while physically crosslinked ones depend on physical interactions to prevent dissolution. These differences in crosslinking also lead to differences in the mechanical properties of hydrogels.

1.4.1.1. Physically Crosslinked Hydrogels

Physically crosslinked hydrogels consist of reversible intermolecular interactions. These interactions include ionic/electrostatic interactions, hydrogen bonding, polymer entanglements, hydrophobic/hydrophilic contacts, crystallization/stereo-complex creation, metal coordination, and π-π stacking.[30]

There are several advantages and disadvantages of physical cross-linking. One of the advantages is that it is considered safer than chemical crosslinking because it does not require a crosslinking chemical. Additionally, thanks to the self-assembly process, physical cross-linked materials per se have the self-healing and injectable properties at room temperature.[30] But, they also have some disadvantages of inflexibility in relation to variables such as gelation time, gel pore size, chemical functionalization, and degradation. Furthermore, because of the physical interactions being reversible, physical crosslinked hydrogels exhibit poor mechanical properties.[31]

1.4.1.2. Chemically Crosslinked Hydrogels

Chemically crosslinked hydrogels are more durable than physical hydrogels due to the strong covalent bonds between polymer chains. Chemical crosslinking can be achieved using small cross-linker molecules, polymer-polymer conjugation, photosensitive agents, or enzyme-catalyzed processes. Chemically crosslinked hydrogels have remarkable advantages of flexibility in gelation time, gel pore size, chemical functionalization, and degradation or dissolution. They typically have strong mechanical

properties and structural integrity. This stable three-dimensional network made by covalent bonds ensures permanence and resistance to environmental changes.[31]

1.4.1.3. Photocrosslinking

Photocrosslinking is forming crosslinking bonds by using a photo-initiator and a light source. It has recently become popular in biomedical applications due to their flexibility. When exposed to UV or visible light, photo-initiators produce free radicals that initiate the polymerization process. These free radicals convert aqueous macromer solutions into hydrogels. A short exposure to low-intensity light, combined with the relevant photo-initiator, allows photopolymerization to occur with minimal negative effects on cells and bioactive molecules. The mechanical properties and swelling behavior of these hydrogels can be easily modified by changing the photocurable moiety.[32]

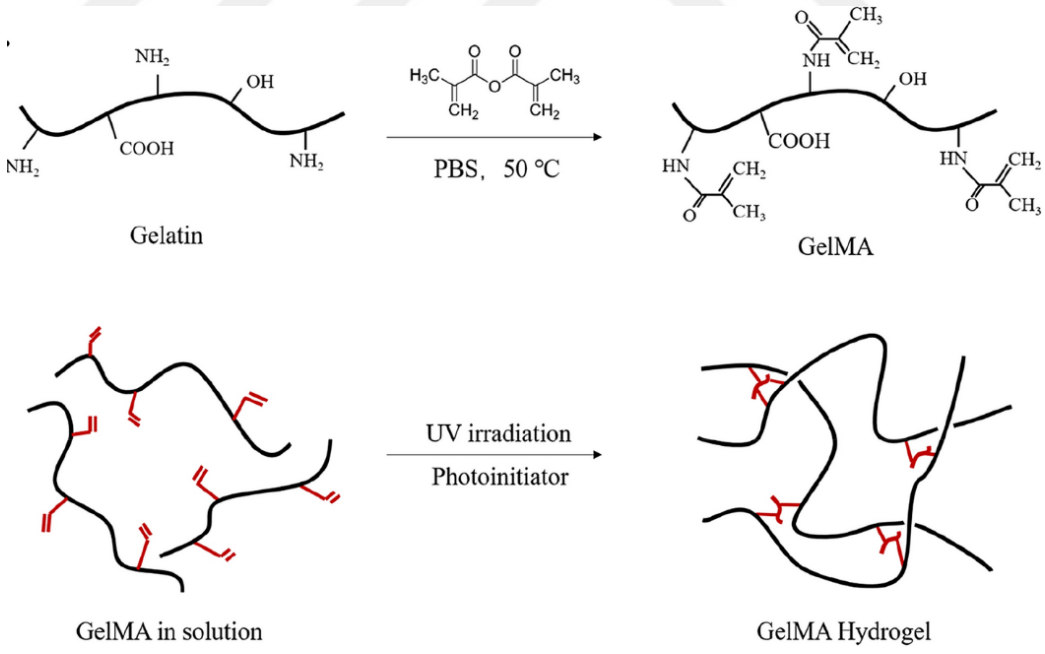

Figure 1.8. Synthesis and Photocrosslinking of Gelatin Methacrylate Hydrogel.[33]

Polymerizable molecules with carbon-carbon unsaturated bonds undergo bond-breaking and addition reactions with the help of initiators and light to form the polymeric

network. Acrylates are an example of these polymerizable groups. Acrylates can be produced by reacting methacrylic anhydride with hydroxyl or amine groups Figure 1.8.[33] Acrylate hydrogels show excellent stability against environmental changes such as temperature and pH variations, and they are not easily modified with functional groups. Thus, they are suitable for applications in biomedicine, where the stability of hydrogel structure is essential for direct interaction with cells or tissues, as well as for biological analyses and other uses. [32]

1.4.2. Hydrogel Polymer Sources

Polymers exhibit intriguing characteristics, such as easy chemical manipulation, which allows for constructing 3D scaffold structures and modifying surface functionalities. Their structural, size, and chemical flexibility make polymers ideal for use as drug delivery systems to enhance wound healing. Consequently, polymers are excellent candidates for use as skin substitutes.[34]

According to their sources according to their source's polymers can be investigated under two groups as: natural polymers and synthetic polymers.

1.4.2.1. Synthetic Polymers

Synthetic polymers are chemically produced polymers with customizable properties that allow for consistent and uniform physicochemical characteristics and stability. These polymers are mechanically stable, free from impurities, and can be degraded under controlled conditions. Various fabrication techniques can be employed to customize synthetic polymers, resulting in a wide range of physical attributes. To create skin substitutes, synthetic and natural polymers can be used in combination [34–36].

Synthetic polymers used for wound dressing applications with a brief information were listed in Table 1.2.

Table 1.2. Properties of Commonly Used Synthetic Polymers for Wound Healing.[34,36,37]

SYNTHETIC POLYMER	PROPERTIES	APPLICATIONS
POLYETHYLENE GLYCOL (PEG)	Hydrophilic, biocompatible, non-immunogenic	Base for hydrogels, controlled drug release
POLYVINYL ALCOHOL (PVA)	Water-soluble, good film-forming ability, excellent chemical stability	Wound dressings, hydrogels for barrier properties and moisture retention
POLY(LACTIC-CO-GLYCOLIC ACID) (PLGA)	Biodegradable, biocompatible, adjustable degradation rates	Hydrogels for controlled drug delivery, tissue engineering scaffolds
POLYURETHANE (PU)	Versatile, durable, varying degrees of elasticity and mechanical strength	Wound dressings, hydrogels for support and flexibility
PLURONIC F127	Triblock copolymers, thermoresponsive, gel-like at body temperature	Hydrogels for drug delivery, wound care due to gelation properties
POLYVINYLPYRROLIDONE (PVP)	Water-soluble, good film-forming properties, adhesiveness	Wound dressings, hydrogels for creating a moist wound environment

1.4.2.2. Pluronic F127

Pluronic F127, with a structure given in Figure 1.9 [38], also known as Poloxamer 407, is a synthetic triblock copolymer characterized by a central hydrophobic segment of polypropylene oxide (PPO) fringed by two hydrophilic segments of polyethylene oxide (PEO). F127 has distinct thermo-reversible gelation properties, compatibility with biological systems, and adaptability, which makes it well-suited for different biomedical uses, such as in wound-healing hydrogel formulations. F127 has a reversible transformation from solution to gel with varying temperatures, being in a fluid state at lower temperatures and converting to a gel state at body temperature (around 37°C). This feature facilitates easy application and in-situ gel formation. F127 is generally non-toxic and has good tolerance by biological tissues; it minimizes the likelihood of adverse responses when employed in wound management. The hydrophilic characteristics of the PEO fringe contribute to moisture retention, which is a critical aspect of wound recovery.[37,39,40]

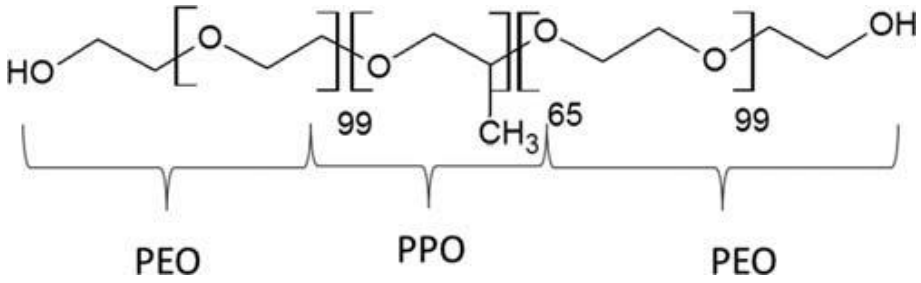

Figure 1.9. Chemical Structure of Pluronic F127.[38]

1.4.2.3. Natural Polymers

Natural polymers are derived from natural sources such as microbial, plant-based material, and animal biomass. These polymers have valuable properties such as biodegradability, biocompatibility, and biological activity, which makes them well-suited for applications in the field of biomedicine. The byproducts of natural polymers are low in toxicity and are absorbed by living organisms, making them a favorable choice. However, natural polymers have limitations, including challenges in controlling their degradation rates and processes.[36] Table 1.3 lists natural polymers commonly used in wound healing applications.

Table 1.3. Properties of Natural Polymers.[34,36,41–43]

NATURAL POLYMER	PROPERTIES	FOUND IN
HYALURONIC ACID (HA)	Highly hydrophilic, viscoelastic, promotes cell migration and proliferation	Connective tissues, skin, synovial fluid
CHITOSAN	Biodegradable, biocompatible, antibacterial properties	Derived from chitin in crustacean shells
ALGINATE	Forms hydrogels in the presence of divalent cations like calcium	Extracted from brown seaweed
COLLAGEN	Supports cell attachment and growth	Extracellular matrix of animal tissues
GELATIN	Denatured form of collagen, easily processed	Derived from collagen in animal tissues

(cont. on next page)

Table 1.3 (cont.).

SILK FIBROIN	Derived from silkworm cocoons, excellent mechanical properties	Silkworm cocoons
PECTIN	Forms gels in the presence of calcium ions	Plant cell walls, especially in citrus fruits and apples
KERATIN	Derived from human hair, wool, and feathers; promotes cell adhesion and proliferation	Hair, wool, feathers
SILK SERICIN	Water-soluble protein, promotes moisture retention, and has antioxidative properties	Coating on silk fibroin fibers from silkworm cocoons

1.4.2.4. Keratin

Keratin is a fibrous protein found in hair, wool, feathers, and the skin's outer layer (epidermis). From the several forms of keratin, wool keratin from sheep wool has numerous advantages in the manufacture of wound healing hydrogels. Wool keratin, a natural protein, is biocompatible and less prone to elicit adverse responses than synthetic polymers, ensuring patient safety. Also, having the ability to induce cell matrix interactions due to the peptide sequence groups of Arg-Gly-Asp (RGD), Leu-Asp-Val (LDV), which play a significant role in cell attachment.[44]

Wool keratin has a high cysteine amount, making up 7%–20% of the total amino acid content, contributing to the fibers' strength via numerous intra- and intermolecular disulfide (S–S) bonds, including sulfhydryl–disulfide (SH–SS), hydrogen bonding, and Coulombic linkages that facilitate cystine formation through disulfide bridges. Cysteine, one of the four sulfur-containing amino acids (along with methionine, homocysteine, and taurine), is incorporated into proteins along with methionine. Unlike methionine, cysteine residues in keratin polypeptides have a chemically reactive thiol (–SH) group at physiological pH (~7.0), forming disulfide bridges (Cys-S–S-Cys) when oxidized. These S–S interactions are crucial for protein structure, folding pathways, and stabilization of the three-dimensional keratin subunits, providing resistance to thermal, chemical, and enzymatic reactions (Figure 1.10). [45]

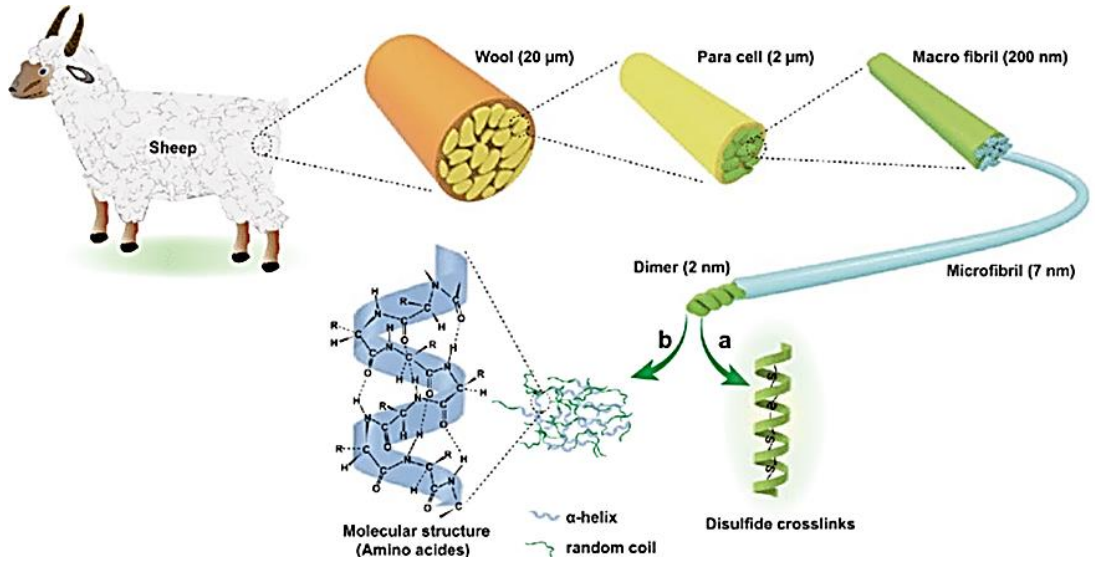

Figure 1.10. Schematic representation of Wool to Keratin.[46]

Wool keratin's customizability enables it to be mixed with a variety of polymers and medicinal ingredients, resulting in hydrogels with qualities customized to specific wound types. Furthermore, using wool keratin generated from sheep wool is a sustainable strategy that makes use of natural, renewable resources.

1.5. Multifunctional Wound Dressing Hydrogels

Hydrogels were originally only used as wound dressings for essential physical isolation and moisturizing. However, as clinical requirements for wound repair increased, more and more demands were made of material performance, and as basic research continued, more hydrogel dressings with improved single- or multiple-biological functions started to emerge.[47] Hydrogels were loaded with bioactive materials such flavonoids [48], herbal extracts [49,50], growth factors [51], antibiotics [52], and nanoparticles [53,54] to promote the healing process of chronic wounds. Hydrogels' network structure enables the entrapment of bioactive materials within the three-dimensional crosslinked matrix, facilitating controlled and systematic drug release.[55]

1.5.1. Gallic Acid

Gallic acid, also known as 3,4,5-trihydroxybenzoic acid, is one of the most prevalent phenolic acids found in plants. It is a crystalline substance that is white or slightly yellow and finds wide use in the food and medicinal areas. Many chromatographic techniques have been used to isolate gallic acid from a variety of plant species, including Quercus and Punica species. However, from an industrial perspective, gallic acid is generated by hydrolyzing tannic acid with the enzyme tannase. [56]

Gallic acid has been found to have antioxidant, anti-inflammatory, and anti-diabetic effects. In surgical wounds, gallic acid has been shown to accelerate the process of re-epithelialization and improve healing. It is an efficient antibacterial agent for bacteria isolated from wounds. It has the potential to be developed into a helpful agent for the treatment of wounds because of its advantageous qualities. [57]

1.5.2. Curcumin-Lysine Carbon Dots

Nanomaterials with dimensions ranging from 1 to 100 nanometers in at least one direction have been effectively used in multi-functional hydrogel formulations. They can be zero-dimensional, one-dimensional, two-dimensional, or three-dimensional. Compared to bulk solids, these materials have distinct features in optics, heat, electricity, magnetism, mechanics, and chemistry, which makes them very adaptable. Carbon dots (CDs), carbon-based zero-dimensional nanomaterials, are nano-size for all three dimensions and characterized by spherical morphology with less than 10 nm. CDs were discovered in 2004, whereas single-walled carbon nanotubes were purified by Xu et al. from the University of South Carolina. [58,59]

The unique structure and composition of the CDs offer several beneficial properties, including a large specific surface area, high water solubility, high chemical stability, low toxicity, photocatalytic activity, stable fluorescence, and excellent biocompatibility. Additionally, they can be antioxidant, antimicrobial, and biodegradable, depending on the precursor used. [58] The CD's functional and biological potential is strongly related to the nanomaterial core structure. Specifically, the functional groups

were exposed to the CD surface. Furthermore, the selection of precursors and techniques used in the production process directly affect the structure of CDs. Therefore, structurally distinct nanoparticles can be produced by slight variations in the types of precursors, solvents, and synthesis methods. [60] In this thesis, curcumin and lysine were used to prepare keratin hydrogel formulations due to their following properties.

Curcumin is considered as a multi-functional compound with antioxidant [61], anti-inflammatory [62], and broad-spectrum antibacterial properties [63], as well as potential anticancer effects. [62] However, the limited solubility of curcumin, particularly in water, presents a challenge for its pharmaceutical application. This limitation may be solved by modifying its structure or conjugating it with other compounds. [64,65]

Lysine is one of the 22 amino acids found in the structure of proteins. This polar amino acid, which has desirable properties such as supporting cell proliferation in the human body, must be obtained externally, unlike arginine, which has similar properties and can be produced naturally in the body. The polar structure (positively charged) of lysine also gives it hydrophilic properties. [66–68] Lysine is also found in the amino acid sequence of naturally occurring antimicrobial peptides (AMPs). These AMPs provide an innovative drug option against antibiotic resistance, which has become widespread today, and they can replace antibiotics.[69,70]

Thus, combining curcumin and lysine in a CD platform can be beneficial in promoting wound healing due to the water solubility, cell proliferation, and antimicrobial properties of lysine, as well as curcumin's antioxidant and antibacterial properties.

1.6. Scope of the Thesis

The main objective of this MSc. Thesis is to develop photo-crosslinked wool keratin-Pluronic F127 hydrogels loaded with gallic acid and curcumin-lysine carbon dots for wound healing applications.

The contents of each chapter are outlined below:

- Chapter 1: Introduction

This chapter provides information about wool keratin, Pluronic F127, gallic acid and curcumin-lysine carbon dots. It introduces the problem statement and outlines the structure of the thesis.

- Chapter 2: Literature Review

A review of existing literature related to wound healing materials, keratin, Pluronic F127, hydrogels, and nanomaterials is presented in this chapter. It covers the current state of research and identifies gaps that this study aims to fill.

- Chapter 3: Materials and Methods

This chapter details the materials used in the research and the experimental methods employed. It describes the preparation and characterization of keratin-Pluronic F127-based hydrogels, Curcumin-Lysine Carbon Dots, Gallic acid-loaded hydrogels, and GACD-loaded hydrogels for wound healing.

- Chapter 4: Results and Discussion

The results obtained from various experiments are presented in this chapter. It includes data on physical and chemical properties of hydrogels, their swelling behavior, mechanical properties, and biological activities.

Data were analyzed and discussed in the context of the research questions and hypotheses. The discussion connects the results to the existing literature, highlighting the implications and significance of the findings.

- Chapter 5: Conclusions and Future Work

The final chapter summarizes the key findings of the research, highlighting the contributions to the field of wound healing materials. It reiterates the significance of the study and its potential impact on future research and clinical applications.

- References

A complete list of all the sources cited throughout the thesis is provided at the end.

CHAPTER 2

LITERATURE REVIEW

In this chapter, a literature review of the hydrogels used in wound-healing applications and wound healing properties of gallic acid, and carbon dots were present.

2.1. Hydrogels in Wound Healing

Wang and coworkers worked on extraction of keratins from chicken feathers and used these keratins to prepare a hydrogel to observe the in vivo wound healing. Feather keratin was extracted with reducing conditions using the Shindai method. The process comprised of three steps: ethanol pretreatment, hydrochloric acid pretreatment, and deoxidization with 2-mercaptoethanol. Hydrogels were prepared in three different concentrations (10, 15, 20% (w/v)) by adding H_2O_2 to trigger the formation of disulphide bonds and incubated at 37 ºC overnight.[71]

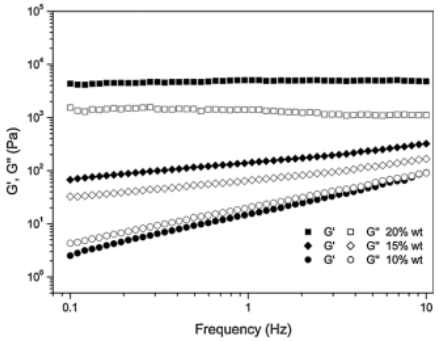

Figure 2.1. Frequency sweep data of self-assembly keratin hydrogels.[71]

Viscoelastic responses of the hydrogel samples were investigated using oscillatory frequency sweep studies at 25°C, ranging from 0.1 to 10 Hz. As keratin concentrations

increased from 10% to 20% of total weight, the hydrogels' moduli increased noticeably. The 10% keratin mixture showed a frequency-dependent elastic modulus (G') that was lower than the viscous modulus (G") over the whole frequency range, indicating that the mixture functions like a viscous liquid at this concentration. However, independent of frequency, G' exceeded G" confirming the formation of hydrogels at 15% and 20% concentrations (Figure 2.1).

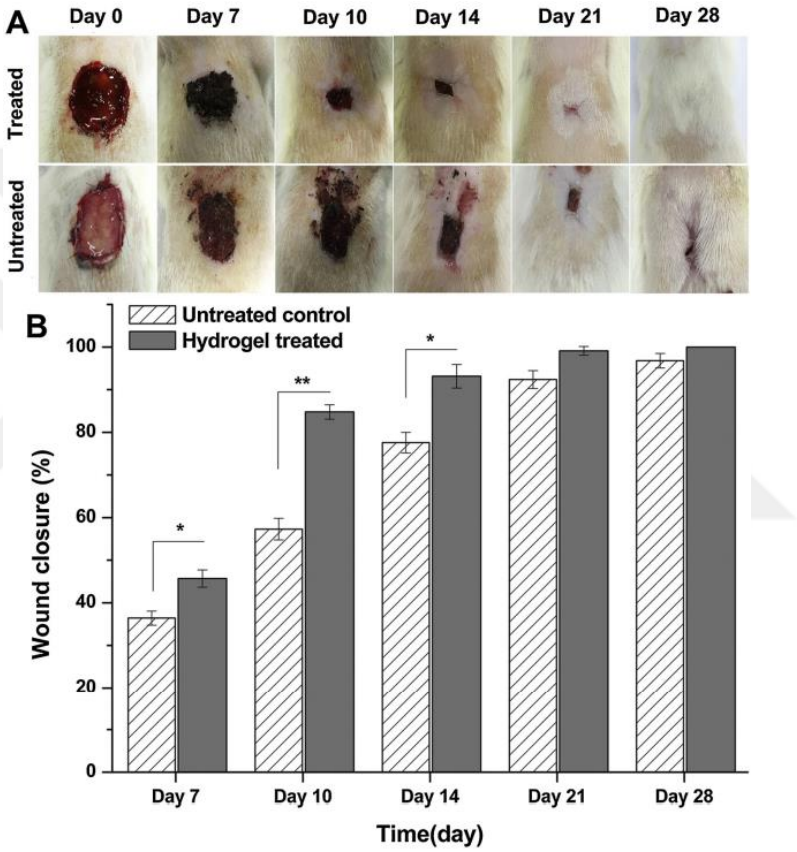

Figure 2.2. In vivo wound healing study of keratin hydrogels.[71]

In vivo wound healing, shown in Figure 2.2 hydrogel treated wounds were enclosed faster than the untreated wounds. Which leads to the result of keratin hydrogels could be used for biomaterial applications, specifically for the promotion of effective wound healing.[71]

Stubbe and coworkers used gelatin to form photocrosslinked hydrogels to support wound healing. Gelatin has a thermo-reversible behavior at body temperature, making it

challenging for biomaterials. To overcome this problem, Stubbe and coworkers used photochemical crosslinking to form gelatin hydrogels. For □hotocrosslinking, gelatin chemical structure requires cross-linkable moieties such as methacryloyl functionalities, which are photo-responsive upon adding a photoinitiator. In their study, different photocrosslinkable forms of gelatin, gelatin methacrylate (Gel-MA), gelatin acrylamide (Gel-AA), and gelatin pentenamide (Gel-PE) were prepared using the reactions in Figure 2.3 and the hydrogel properties were investigated.[72,73]

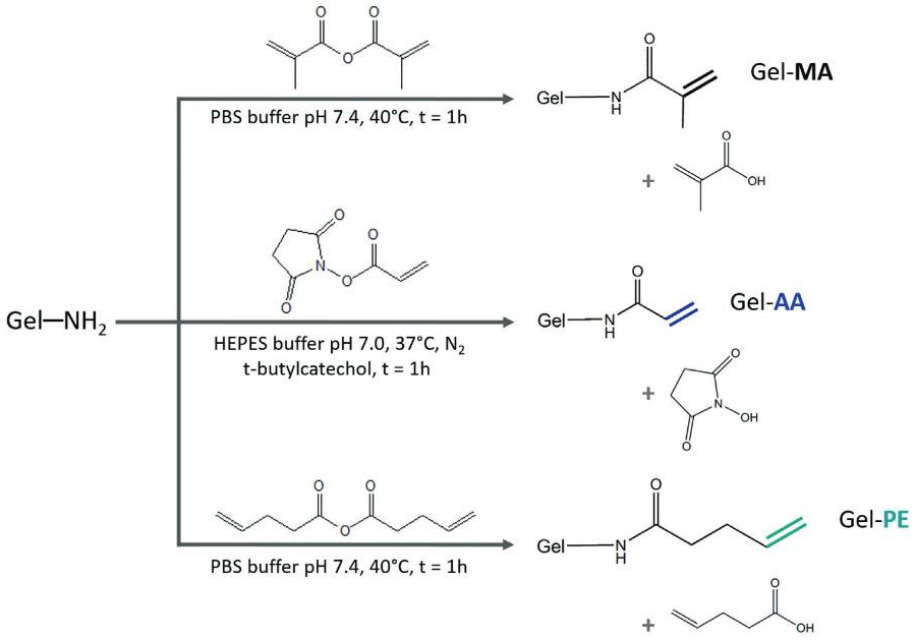

Figure 2.3. Preparation of gelatin derivatives[72]

The hydrogels were prepared using a UV light (λ_{max} = 365 nm, 6 mW/cm^{-2}) and the photoinitiator, Irgacure 2959. In vitro cell viability and proliferation data results of these hydrogels are presented in Figure 2.4. Both Gel-MA and Gel-AA hydrogels exhibited high cell viability and cell proliferation. Rheological results of the hydrogels given in Figure 2.5 show that G' (storage modulus) values increase with increasing DS, and the highest storage modulus value was obtained for the Gel-MA hydrogel.[72]

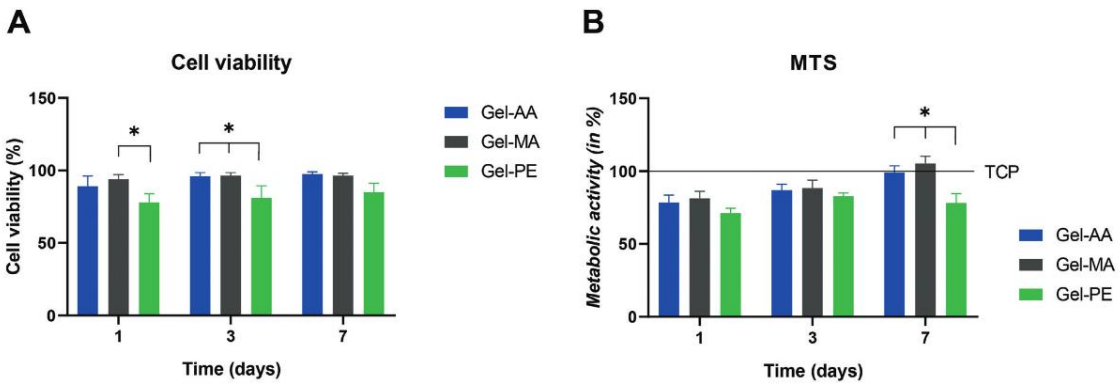

Figure 2.4. In vitro biological analyses of gelatin derivative hydrogels. (A) Live/Dead assay results. (B) Proliferation results.[72]

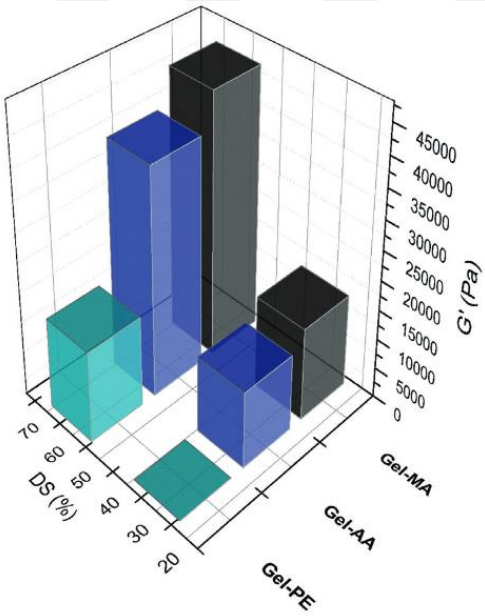

Figure 2.5. Storage moduli G' values of photocrosslinked gelatin derivative hydrogels[72]

Sharun and coworkers studied the therapeutic effect of pluronic F127 on wound healing using in vivo experiments. Adipose-derived stromal vascular fraction (AdSVF), mesenchymal stem cells (AdMSC), and conditioned media (AdMSC-CM) and their encapsulated froms with pluronic F127 hydrogels were investigated for the repair of wounds in a rabbit model Figure 2.6. There were total of eight groups of different treatment protocols investigated.

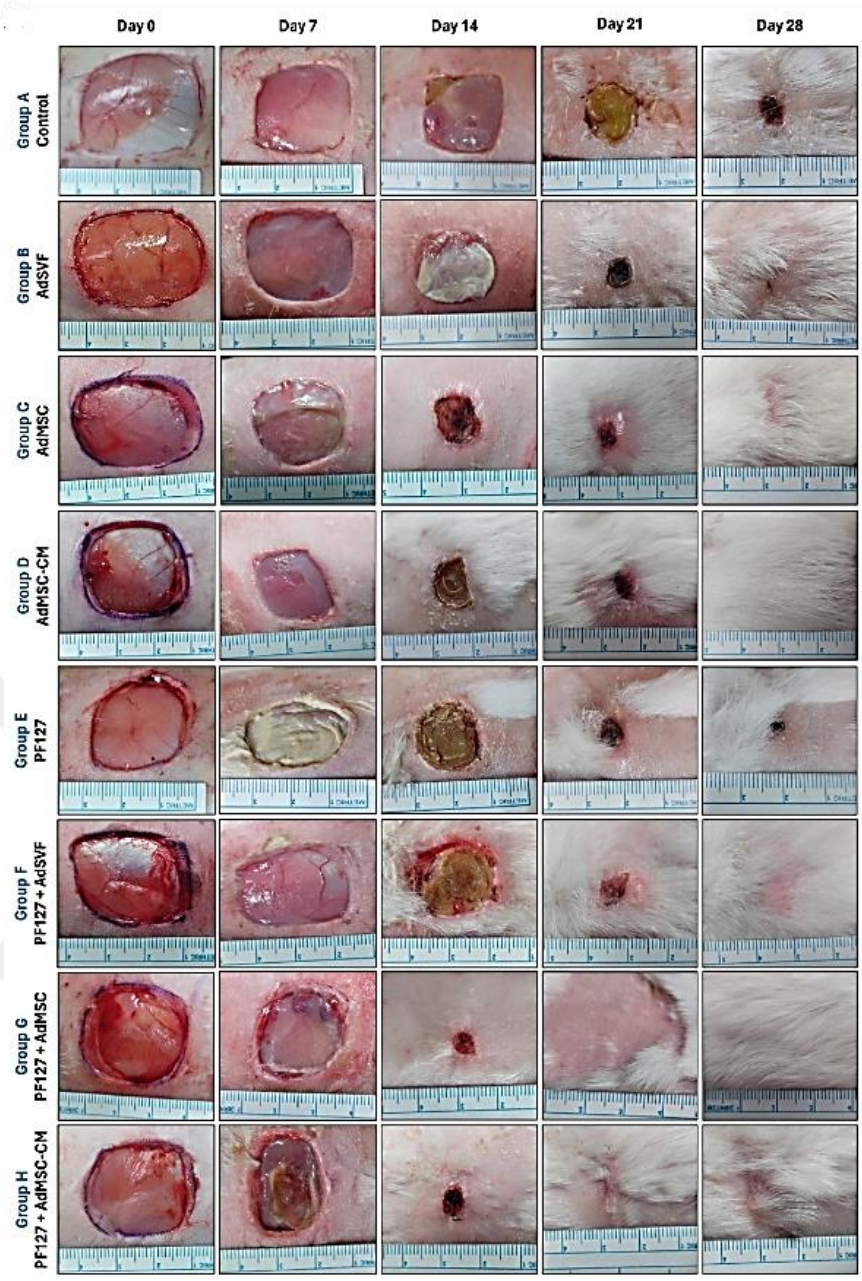

Figure 2.6. Wound photographs of different groups (Groups A-H) at different time intervals (days 0, 7, 14, 21, and 28) showing the progression of wound healing. [74]

2.2. Wound Healing Properties of Gallic Acid and Carbon Dots

Riaz and coworkers prepared gallic acid (GA) loaded agarose (AG) and l-phenylalanine (LPF) multifunctional hydrogels. The hydrogels were obtained by mixing a fixed ratio of LPF and AG molecules (7:3), with varying content of GA to make three

different hybrid hydrogels named LPF-AG-GA1 (1 wt% GA), LPF-AG-GA2 (2 wt% GA) and LPF-AG-GA3 (3 wt% GA). The antioxidant abilities of hydrogels were evaluated by DPPH and ABTS free radical scavenging analyses. Figure 2.7 shows that DPPH and ABTS solutions are decolorized by increasing the amount of GA, indicating increased antioxidant properties. UV absorbance values and the scavenging percentages calculated from those values also support the decolorization. Gram-negative (*E. coli* and P. aeruginosa) and Gram-positive (*S. aureus*) bacterial strains were used for the antibacterial tests of the hydrogels. Disk diffusion results in Figure 2.8 indicate that even 1% of GA can inhibit the growth of *S. aureus* and *P. aeruginosa*, but higher amounts of GA are required to prevent the formation of *E. coli* colonies.[75] Thus, the incorporation of GA imparts antioxidant and antibacterial properties to hydrogels.

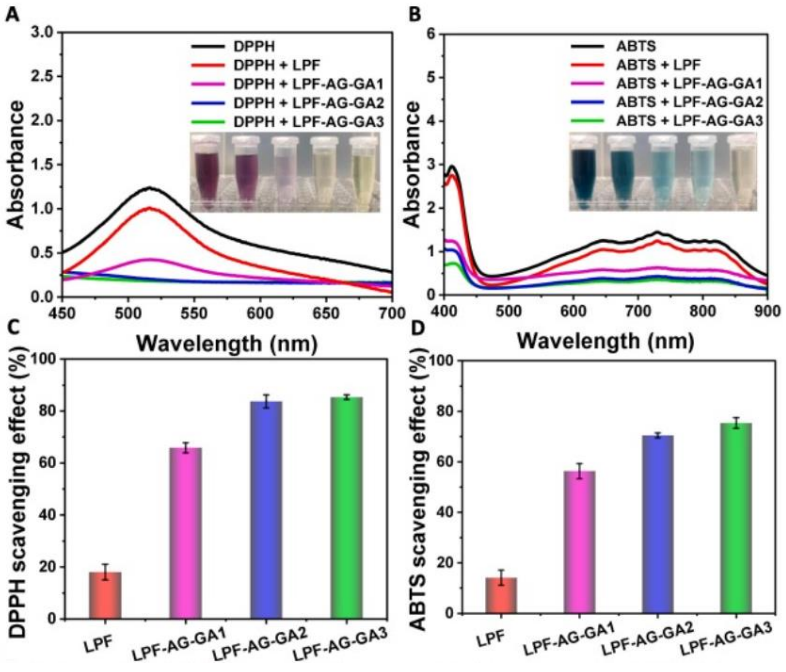

Figure 2.7. Antioxidant efficiencies of GA loaded hydrogels. [75]

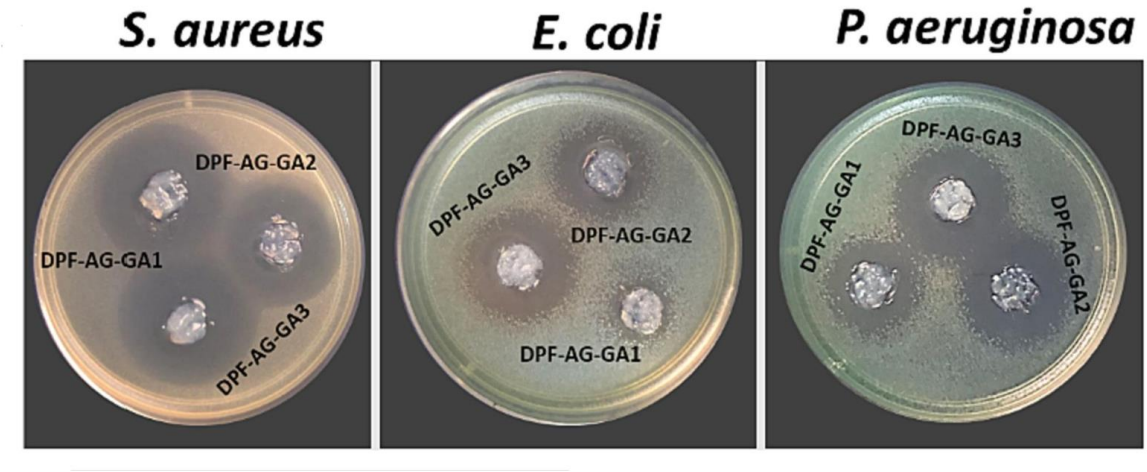

Figure 2.8. Hydrogel antibacterial test images of different GA. [75]

Li and coworkers studied the antibacterial properties, cytotoxicity, and bacteria-infected wound healing efficiencies of carbon dots (CD) synthesized from L-lysine and L-arginine. CDs were synthesized via the pyrolysis method, in which L-lysine or L-arginine was placed inside a furnace to reach the temperature of 240°C and kept at this temperature for 3 hours. The residue was dissolved in ultrapure water, and the supernatant was dialyzed against water and then freeze-dried for analysis. The antibacterial properties of CDs were studied against *S. aureus*. A biofilm formed by *S. aureus* was prepared, and different concentrations of Lys-CQDs and Arg-CQDs were added to the biofilm. After 48 hours of incubation, the untreated group of *S. aureus* generates a diverse and robust biofilm. CQDs greatly diminish bacterial biofilms, resulting in a detached island-like morphology. Confocal scanning laser microscopy (CLSM) confirms that biofilms thin with increased CQD concentration. The cytotoxicity of CDs was investigated using NIH-3T3 cells. The survival rate of cells increased with the addition of CDs and continued to increase within a specific concentration range, as shown in Figure 2.9. After seven days of culture, the cell viability values in both the Lys-CQDs and Arg-CQDs groups increased by nearly seven times when compared to the control. Mouse models were used for the bacteria-infected wound healing studies. Bacteria strains that infected the wound area were *S. aureus* and *E. Coli*. In Lys and Arg CQDs, there were significant improvements in wound closure, as seen in Figure 2.10. Thus, it was shown that lysine and arginine CDs have potential in wound healing applications with minimal cytotoxicity.[76]

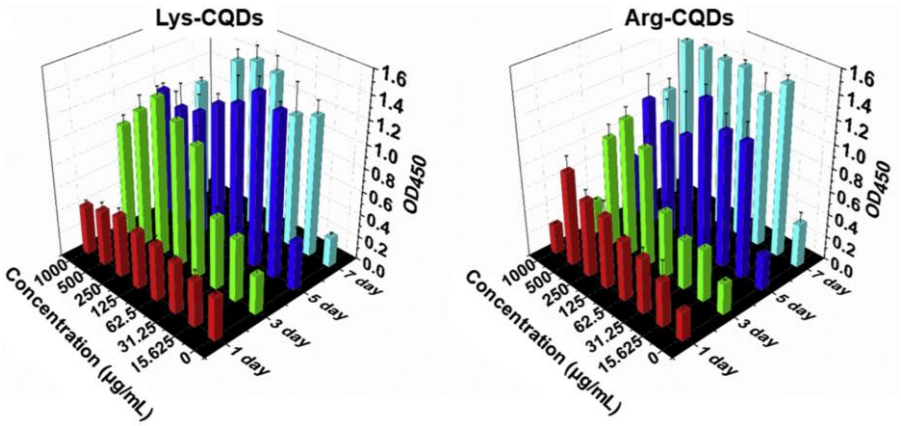

Figure 2.9. Cytotoxicity of CDs on NIH-3T3 cell line. [76]

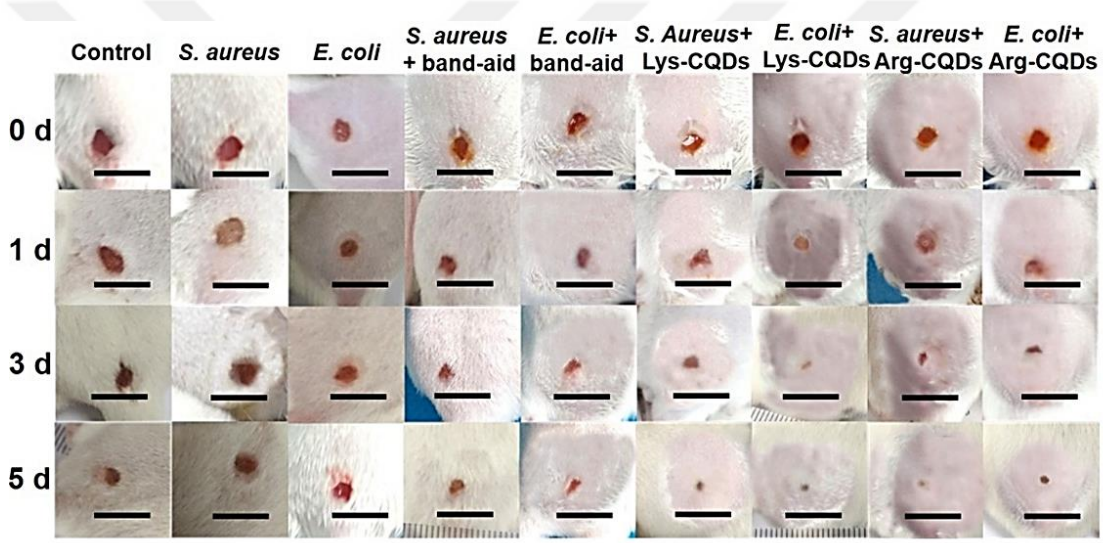

Figure 2.10. Photographs of wounds on the backs of mice from nine groups at different times. (scale bars,10 mm)[76]

CHAPTER 3

MATERIALS AND METHODS

3.1. Materials

Wool, chloroform (Sigma-Aldrich) and methanol (Sigma-Aldrich) were used for the extraction of fat from the wools. Peracetic acid solution (Merck-Supelco), Tris-base (Merck), Tris-HCl (Sigma-Aldrich) and regenerated cellulose tubing dialysis membrane (SERVA, MWCO ~12000-14000) were used for extraction and isolation of the keratoses. Sodium phosphate dibasic (Na_2HPO_4, Merck), potassium phosphate monobasic (KH2PO4, Merck), NaCl (Sigma-Aldrich) and KCl (Panreac) were used for phosphate buffer saline (PBS) preparation. Sodium hydroxide (Sigma-Aldrich) and hydrochloric acid (Merck) were used to adjust pH of the solutions. Methacrylic anhydrite (Sigma-Aldrich), Pluronic F127 (Sigma-Aldrich), triethylamine (TEA, Sigma-Aldrich), and diethyl ether (DEE, Sigma-Aldrich), were used for methacrylation reaction and purification of keratoses and Pluronic. 2,4,6-trinitrobenzene sulfonic acid solution (TNBSA, 5% w/v in H_2O, Sigma-Aldrich) and sodium tetraborate (Sigma-Aldrich) were used for obtaining the methacrylation degree of keratoses. Curcumin (Merck- Millipore), and L-Lysine (Carl Roth) were used for carbon dot synthesis. 2-Hydroxy-4′-(2-hydroxyethoxy)-2-methylpropiophenone (Irgacure 2959, Sigma-Aldrich) was used as photoinitiator and 365 nm UV-Lamp for photo-polymerization. DPPH (TCI- Tokyo Chemical Industry) and ethanol (Sigma-Aldrich) were used for antioxidant analysis. For the cell studies, DMEM cell culture medium (high glucose) (Gibco), fetal bovine serum (FBS, European grade) (Gibco), L-Glutamine (Serox), Penicillin-Streptomycin (Serox), 0.25% trypsin-EDTA solution (Gibco), Trypan blue solution (5 mg/ml, Biological Industries), and Cell-Quant™ AlamarBlue Cell Viability Reagent (ABS Bio) were used. For the antimicrobial disc diffusion analyses, Agar (Sigma-Aldrich), Mueller Hinton Broth (Merck- Millipore), Oxoid™ Amoxycillin Antimicrobial Susceptibility discs (Thermo-Fisher Scientific), and Oxoid™ Blank Antimicrobial Susceptibility discs (Thermo-Fisher Scientific) were used.

3.2. Methods

3.2.1. Extraction of Keratose Proteins (KTS) from Wool

The keratose proteins were extracted following the procedure outlined by Yalçın and Top (2022). This involved cleaning, defatting, and oxidizing wool samples cut into small pieces using a 1.8% (w/v) peracetic acid solution. The oxidation process was completed according to the method described by Pakkaner et al. (2019) followed by dialysis using a ~14000 MWCO dialysis membrane and freeze-drying. The samples were then stored at -20°C for future use.

3.2.2. Synthesis of Methacrylated Keratose (KTSMA) and Methacrylated Pluronic (F127MA)

To the extracted keratose proteins dissolved in 10 mM PBS buffer (5 mg/ml), methacrylic anhydride was added, and the reaction proceeded at 50°C for 3 h. After the reaction, the solution was dialyzed using a ~14000 MWCO dialysis tubing membrane for 5 days. The solution was freeze-dried after adjusting its pH to 7.5-8, and the methacrylated keratose samples were stored at -20°C for future use.

The protocol outlined by Lin-Gibson et al. (2004) was adapted for the methacrylation of Pluronic F127. 1 g Pluronic F127 was dissolved in 0.944 mL of methacrylic anhydride, and 0.04 mL of TEA was added to the mixture. The solution was placed in a 50°C shaking incubator for 3 days. After this period, the solution was precipitated into diethyl ether three times and freeze-dried for future applications.

The methacrylation degree of KTSMA was determined by using the TNBSA (2,4,6-trinitrobenzene sulfonic acid) assay, with the procedure given by Snyder and Sobocinski (1975). A known amount of KTS and KTSMA was dissolved in a 0.01 M sodium tetraborate solution at pH 9.3. Then, the protein solution mixed with 25 µL of 0.03 M TNBSA solution was incubated at room temperature for 30 minutes. The absorbance of the resulting mixture at 420 nm was measured with the instrument of UV-Vis spectrophotometer (Shimadzu UV-2450). The amine concentration was determined

using an attenuation coefficient of 11.2 x 10^3 cm-1 M^{-1} at 420 nm, as given by Snyder and Sobocinski (1975). The methacrylation degree was calculated based on the reduction in amine concentration using the following equation:

$$\%\ Methacrylation = \left(1 - \frac{mmol\ amine\ in\ 1\ mg\ KTS}{mmol\ amine\ in\ 1\ mg\ KTSMA}\right) * 100 \qquad (3.1)$$

Functional groups of the samples were analyzed using FTIR-ATR spectroscopy using the wavelength range of 4000–400 cm^{-1}, 32 scans and a resolution of 2 cm^{-1}. The spectra were acquired using a Perkin Elmer – UATR TWO instrument. Proton Nuclear Magnetic Resonance (1H NMR) spectroscopy of the F127MA was taken on MERCURY plus-AS 400 instrument at Ege University Central Research Test and Analysis Laboratory Application and Research Center. The NMR data were analyzed using MestreNova software.

3.2.3. Preparation of KTSMA and F127MA Hydrogels

Hydrogels were prepared in three different compositions and two different concentrations. 4% KTSMA (K4), 7.5% KTSMA (K7.5), and 4% KTSMA combined with 3.5% F127MA (KP7.5) hydrogels. These hydrogels were formed by initially dissolving the photo-initiator, irgacure 2959, in PBS at a ratio of 0.5% (w/v). Then, the polymers, KTSMA and F127MA, were added, and the solution was homogeneously mixed. Subsequently, the mixture was poured into molds with 2 mm height and 6 mm diameter and crosslinked using a UV lamp (6 mW/cm2, 365 nm wavelength) for 5 minutes.

3.2.4. Characterization of KTSMA and F127MA Hydrogels

Oscillatory rheology tests were conducted at 25°C using a Thermo Fisher Scientific HAAKE MARS model rheometer equipped with a 35 mm diameter stainless steel parallel plate. The hydrogels were placed on the plate with a 0.5 mm gap distance. The frequency for the strain sweep experiments was set at 10 Hz, and the frequency sweep tests were performed at 0.2% strain. Each set of experiments consisted of two independent measurements.

For the swelling experiments, 200 µL of hydrogel was prepared in deionized water, with three replicates for each sample, and then lyophilized. The dry weight (W_d) was determined by weighing the freeze-dried hydrogel. Then, the lyophilized hydrogel was immersed in 5 mL of PBS. At specific time intervals (3, 6, 24, and 48 hours), the excess water was removed from the samples, and the samples were weighed again to determine the weight of the swollen hydrogel (W_s). The swelling ratios of the hydrogels were calculated using the equation given by Yalçın and Top (2022).

$$Swelling\ Ratio\ at\ time\ t = \frac{W_t - W_d}{W_d} \tag{3.2}$$

The degradation kinetics were determined through mass loss measurements following the protocols outlined by Galler et al. (2010) and Li et al. (2015). Firstly, the empty vial was weighed. Subsequently, 200 µL of hydrogel was prepared in the same vial, 5 ml PBS was added, and incubated at 37°C for 3 hours. With the removal of PBS from the hydrogel, the initial weight (W_o) of the swollen gel was recorded. Then, 5 ml of PBS was added, and the vials were incubated at 37°C. At the end of each day, the PBS solution was withdrawn from the surface and the weights of the remaining hydrogels were measured (W_t). This process was repeated for 28 days, and the remaining mass percentage of the hydrogels were calculated using a specific formula and plotted against time.

$$\text{Remaining Mass Percentage} = \frac{W_t}{W_o} \times \% 100 \quad (3.3)$$

Scanning electron microscopy (SEM) was employed to examine the pore structure of the hydrogels. The hydrogels were prepared in deionized water and then freeze-dried before the analysis. Then, the samples were coated with a thin layer of gold. The study was conducted using an FEI Quanta 250 FEG instrument.

The interactions between hydrogels and cells were investigated by studying the proliferation of 3T3 mouse fibroblast cells with the Alamar Blue assay. K4, K7.5, and KP7.5 hydrogels were prepared and placed in a 96-well black plate. The hydrogels were conditioned in DMEM at 37°C with 5% CO_2 for 24 hours. After conditioning, 2500 cells per well were cultured on the hydrogels, and empty tissue culture-treated polystyrene (TCP) wells were used as control samples. All samples were incubated under the same conditions of 37°C and 5% CO2. Fluorometric readings, with an excitation at 530 nm and emission at 590 nm, were taken on the first, third, and seventh days using a Thermo Fisher Varioskan Flash microplate reader. The relative proliferation rate was determined using four replicates for each hydrogel and TCP. Relative proliferation rate was calculated by the following equation:

$$Relative\ Proliferation\ Rate = \frac{Emmision\ of\ Hydrogel}{Average\ Emission\ of\ the\ TCPS\ at\ Day\ 1} \quad (3.4)$$

3.2.5. Synthesis of Curcumin and L-Lysine Carbon Dots

In this study, curcumin-lysine carbon dots were synthesized using two different curcumin-to-lysine ratios. The amount of curcumin used was kept constant at 0.4 g in both samples, while the amount of lysine was used as 2 g and 0.8 g for CL1 and for CL2 samples, respectively. The specified amounts were mixed using a mortar and pestle, then transferred into a crucible and placed in a furnace. The mixture was heated to 250°C with a heating rate of 10°C per minute from room temperature then kept at that temperature

for 3h and allowed to cool to room temperature. The control groups, curcumin and lysine carbon dots were synthesized using the same procedure. After cooling, the samples were dissolved in ultra-pure water and subjected to sonication for 1 hour to ensure complete dissolution. The resulting solutions were centrifuged, and the supernatant was collected. Concentration calculations of the supernatants were performed by freeze-drying a known volume and weighing the residue.

3.2.6. Characterization of Curcumin and L-Lysine Carbon Dots

Thermogravimetric analyses (TGA) were carried out using the Shimadzu TGA-51 instrument. The analyses were performed in a dry air environment between room temperature and at 800ºC, with a heating rate of 10 C/min.

The FTIR-ATR analyses of the freeze-dried samples were conducted using a scan number of 32 and a resolution of 2 cm^{-1}, between 400 to 4000 cm^{-1}. The spectra were collected using a Perkin Elmer – UATR TWO instrument.

X-ray diffraction (XRD) analyses were performed of the samples using a Bruker D8 ADVANCE model diffractometer. XRD patterns were recorded between 2θ range of 10º and 80º with a scan rate of 0.08 degree/s.

A UV-Vis spectrophotometer (Shimadzu UV-2450, Tokyo, Japan) and PL analyses were conducted for optical characterization of CDs.

The particle size analyses of the supernatant samples were conducted using the Zeta-Sizer instrument (Dynamic Light Scattering - DLS, Particulate Systems

Cytotoxicity analyses were performed using NIH 3T3 cells. The cells at a density of 10,000 cells per well incubated for 24h and DMEM containing CDs were added to the wells. The cell proliferation was monitored after one day using Alamar blue assay according to the protocol suggested by the manufacturer. Fluorescence values were measured using a Thermo Fisher Varioskan Flash microplate reader.

The antimicrobial properties of the CDs were determined via antimicrobial disc diffusion analyses. 15 µL volumes of the CD solutions were dispensed onto blank Oxoid discs positioned on Petri plates, which had been inoculated with staphylococcus aureus and Escherichia coli bacteria, cultivated on Mueller Hinton Agar. After 24h incubation at 37 degrees Celsius, the zones surrounding the Oxoid discs were measured.

3.2.7. Preparation and Characterization of Gallic Acid Loaded KTSMA Hydrogels

K4 hydrogels containing different concentrations of gallic acid of 0, 0.1, 0.5, and 1 mg/mL, hydrogels were prepared using the same protocol given in Section 3.2.3, and the resulting hydrogels were named K4, K4GA0.1, K4GA0.5, and K4GA1, respectively.

Cytotoxicity tests of gallic acid-loaded hydrogels were done by indirect contact method. The hydrogels (90 µL) were immersed in DMEM solution (2mL) at 37ºC for 24h. The DMEM extraction solutions were then added to the cells at a density of 10,000 cells per well, which had been cultured on the plate the day before. Wells, with only DMEM were utilized as the control group. After 24 h, alamar blue assay was applied.

The antimicrobial test given in section 3.2.8 was used to determine the antimicrobial activity of the GA-loaded hydrogels. The hydrogels (90 µL) with varying concentrations of gallic acid were incubated in PBS (2 mL) at 37ºC for 24h.

The antioxidant properties of the GA-loaded hydrogels were determined using DPPH protocol of He et al. (2023) was followed with some modifications. Firstly, DPPH solution was prepared (1.5 mM) and diluted with ethanol ten times. From this diluted solution 330 µL diluted solution was added to 90 µL hydrogels. For the control group, 90 µL PBS was used instead of hydrogels. The solutions were incubated at dark and room temperature for 1h. Later, the absorbance values at 517 nm were recorded. The scavenging ratio of hydrogels was calculated using the formula given.

$$\text{Scavenging \%} = \left(\frac{(\text{Absorbance of Control} - \text{Absorbance of Hydrogel})}{\text{Absorbance of Control}}\right) * 100 \quad (3.5)$$

3.2.8. Preparation and Characterization of Gallic Acid and Carbon Dot Loaded KTSMA Hydrogels

KP7.5 hydrogels containing 0.5 mg/mL GA and/or 1 mg/mL CL1 were prepared using the protocol given in section 3.2.3. Viscoelastic properties of the hydrogels were determined as described in 3.2.4. Cytotoxicity of GACD hydrogels was determined using the indirect method in section 3.2.7. The antioxidant assay used in section 3.2.7 was applied.

The scratch assay was performed following the procedure of Liang, Park, and Guan (2007). 3T3 mouse fibroblast cells were cultured in a 96-well plate with a density of 10,000 cells per well. The well plate was incubated at 37^{o}C to create a monolayer and a scratch was formed using a P2 pipette tip per well. Then, DMEM was taken out carefully and replaced by the DMEM extraction solution of GACD hydrogels. The photographs of each well before and after the scratch were taken and the. After 24 hours and 48 hours, photographs of each well were taken, and closure of the scratch was observed. 5 replicates were used for each sample.

CHAPTER 4

RESULTS AND DISCUSSION

4.1. Characterization of Photocrosslinked Keratin Based Hydrogels

In this study, three different keratin-based hydrogel compositions were prepared, as given in Table 4.1. Effects of the composition on mechanical properties, swelling, degradation, morphology, and biocompatibility of the hydrogels were investigated. First, methacrylated forms of the keratin and Pluronic F127 were prepared using the reactions described in Figure 4.1 and Figure 4.2.

Table 4.1. KTSMA and F127MA hydrogel compositions.

Notation	Keratin (w %)	Pluronic (w%)
K4	4	0
K7.5	7.5	0
KP7.5	4	3.5

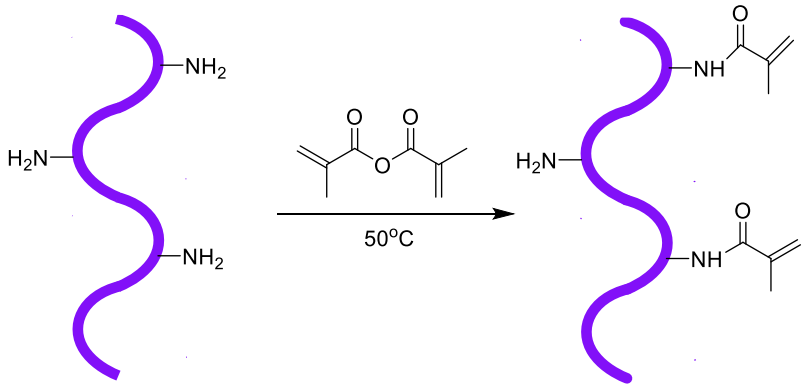

Figure 4.1. Methacrylation reaction of Keratose.

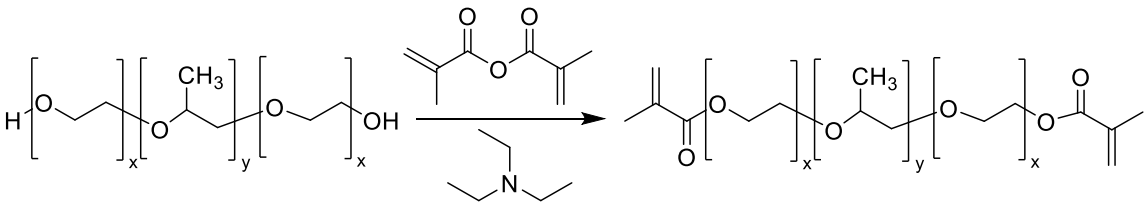

Figure 4.2. Methacrylation reaction of F127.

The methacrylation degree of the KTSMA was optimized using different amounts of methacrylic anhydride (MA) (between 5 µL-400 µL) amounts. The results are given in Figure 4.3. According to these results, the use of 5 µL, 10 µL, and 20 µL MA did not significantly, increase the methacrylation degree monitored via the absorbance at 420 nm. However, between 50 µL and 400 µL, a considerable decrease at 420 nm was observed, confirming methacrylation. Since excess MA can exhibit cytotoxicity, 100 µL MA was chosen for the following experiments.

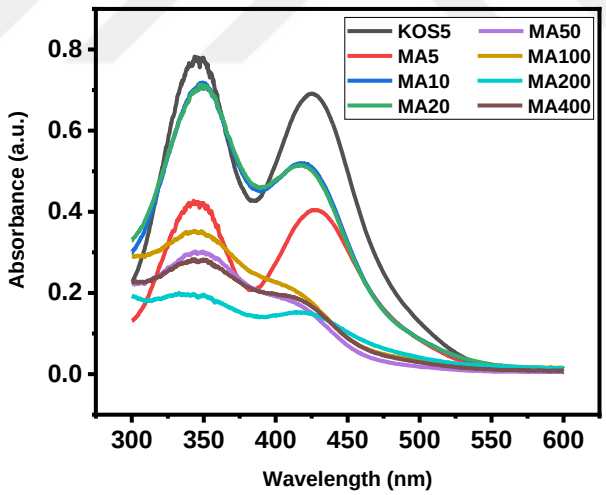

Figure 4.3. UV-Vis spectra obtained for the methacrylation reactions of the keratose different MA amount.

The methacrylation degree of the KTSMA was calculated as 92.5% using the TNBSA assay, with absorbances at 420 nm measured as 0.737 and 0.055, for KTS and KTSMA, respectively. UV spectra of the KTS and KTSMA are given in Figure 4.4.

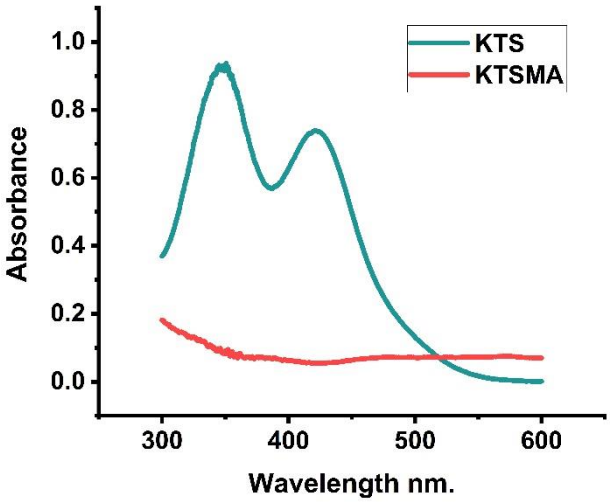

Figure 4.4.UV-VIS spectra of KTS and KTSMA.

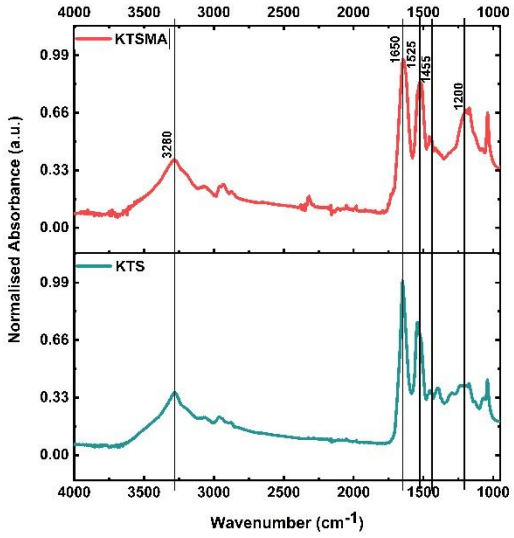

Figure 4.5. ATR-FTIR spectra of KTS and KTSMA.

The ATR-FTIR spectra of the KTS and KTSMA samples (Figure 4.5) display characteristic absorption bands related to the peptide bonds (-CONH-). These peptide bonds exhibit vibrations that result in amide A, amide I, amide II, and amide III. These vibrations appear as the amide A band, at 3280 cm^{-1}, corresponds to the stretching vibration of the NH bond; amide I, mainly associated with the (C=O) stretching vibration

at 1650 cm^{-1}; amide II, linked to the NH bond, 1455 cm^{-1} and 1525 cm^{-1}; and the amide III band, with a sharp band at 1200 cm^{-1}, is attributed to the combination of CN stretching and NH in-plane bending, with some contribution from C-C stretching and C=O bending vibrations. No valuable information was obtained regarding the methacrylation of the KTS in FTIR spectrum as a result of the band overlapping.

The FTIR-ATR spectra of Pluronic F127 and F127MA are given in Figure 4.6. Both spectra indicated fingerprints of Pluronic F127 yet did not provide information for the extent of the methacrylation reaction. For this reason, 1H NMR analysis was conducted and, the NMR spectrum of F127MA is given in Figure 4.7.

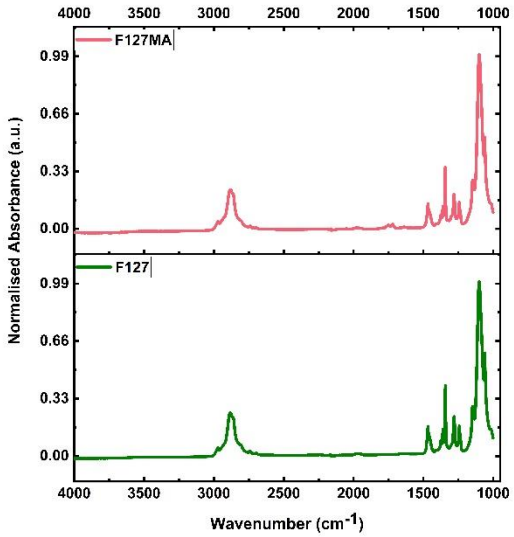

Figure 4.6. ATR-FTIR spectra of F127 and F127MA.

The chemical shifts observed at 3.59 and 3.43 ppm in the NMR spectrum correspond to the backbone protons of PEO and PPO polymer blocks, respectively. The peak obtained at 1.13 ppm is due to the -CH3 group in the PPO side chain. Free methacrylic anhydride protons were observed at 6.27, 5.69, and 2.00 ppm. Methacrylate groups attached to the polymer chain were determined at 6.11, 5.56, and 1.94 ppm, indicating that the methacrylation process was successful. F127 backbone protons adjacent to the methacrylate group were observed at 4.30 ppm.[79]

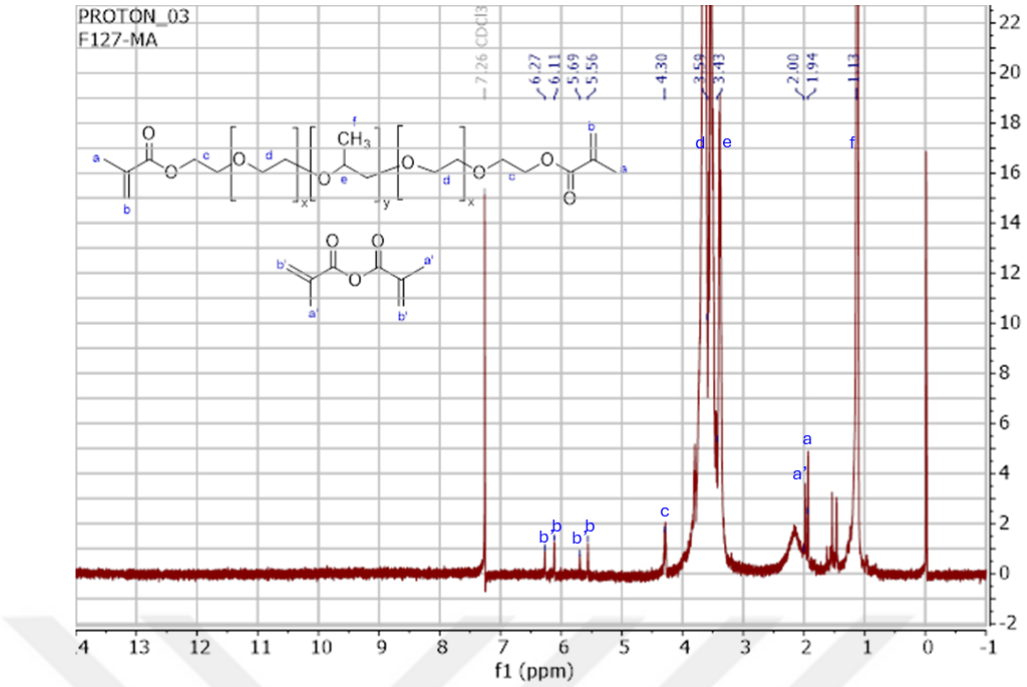

Figure 4.7. 1H NMR spectrum of F127MA.

The frequency and strain sweep data of the KTSMA-F127MA hydrogels were given in Figure 4.8. The frequency sweep analyses were performed between 0.1 Hz and 20 Hz at a constant strain of 0.2%, providing a relative ranking of elastic and viscous properties. G’ (storage modulus) and G” (loss modulus) give insight into the elastic and viscous response behaviors of the hydrogels, with G’ values consistently higher than G” values for all three samples, confirming their gel-like behavior. In all examples, G' and G" values increase as the frequency increases; in other words, gels gain strength. G' values at 10 Hz were obtained as 1380 ± 405, 2640 ± 210, and 3565 ± 720 Pa for K4, K7.5, and KP7.5 hydrogels, respectively. It was observed that increasing the total polymer concentration and using the same amount of F127-MA instead of KRT-MA increased the mechanical properties of the hydrogels. Strain sweep curves show the linear viscoelastic region (LVR). For K7.5 and KP7.5 hydrogels, LVR corresponds to 7% strain. In the K4 hydrogel prepared at lower concentration, LVR extends up to 10% strain, indicating that the hydrogel is more elastic than the others.

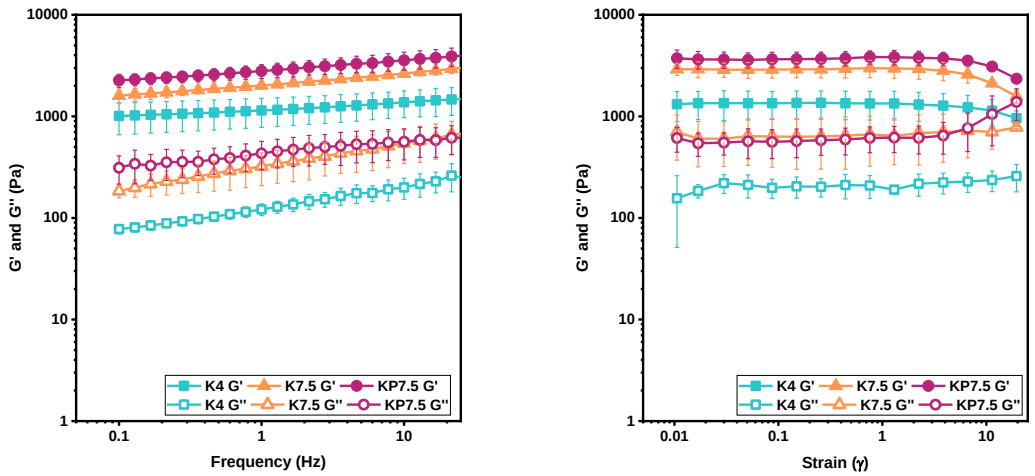

(a) (b)

Figure 4.8. Frequency (a) and strain (b) sweep curves of KTSMA-F127MA hydrogels.

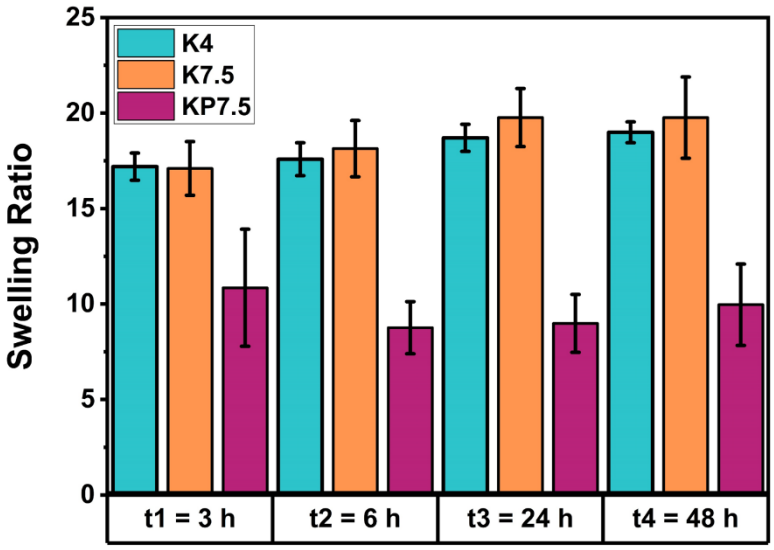

Figure 4.9. Swelling ratios of hydrogels K4, KP7.5, K7.5.

The swelling ratios of hydrogels are given in Figure 4.9. K4 and K7.5 hydrogels, in which only KTS-MA was used in their composition, exhibited a much higher swelling ratio than the KP7.5 hydrogel. The lowest swelling ratio of the KP7.5 hydrogel was due to the hydrophobic polypropylene oxide block in F127. The swelling behavior of the

hydrogels did not change much with time. Therefore, the swelling degree of all hydrogels reaches equilibrium after 3h.

The degradation curves of hydrogels are presented in Figure 4.10. The K7.5 hydrogel experienced a mass loss of approximately 60% in the first five days but maintained a constant mass after that. Both the K4 and KP7.5 hydrogels exhibited a mass loss of approximately 25% over the five-days. In the following days, a mass loss of approximately 5-10% was observed in the K4 and KP7.5 hydrogels. The mass loss in the K7.5 hydrogel can be explained by the high viscosity of the 7.5% KTS-MA solution used to form the K7.5 hydrogel. High viscosity reduces the movement of molecules, thus reducing cross-linking efficiency. the KP7.5 hydrogel precursor solution had a lower viscosity than K7.5. The low mass loss observed despite the high viscosity is due to the hydrophobic PPO chains reducing the water penetration.

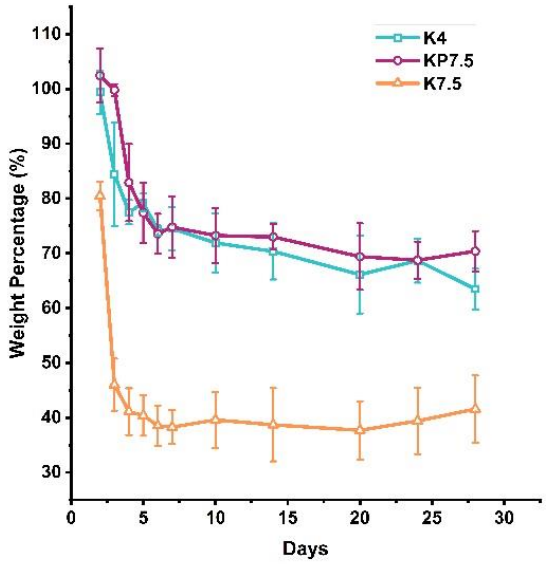

Figure 4.10. Degradation results of K4, KP7.5 and K7.5.

SEM images of freeze-dried hydrogels were given in Figure 4.11. K4 hydrogel exhibited a more irregular pore structure than the others. The high porosity of the KP7.5 hydrogel can be attributed to the reduction of the interaction of keratin chains with each other by the interference of F127MA.

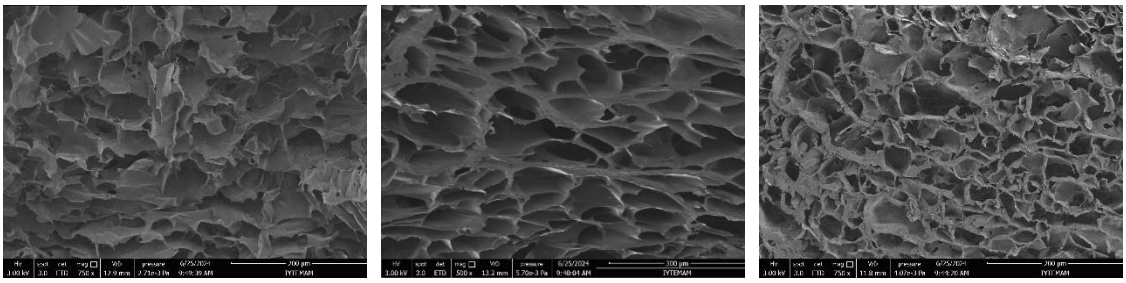

Figure 4.11. SEM images of freeze dried (a) K4, (b) KP7.5 and (c) K7.5 hydrogels. Scale bars: (a), (c) = 200 µm, (b) = 300 µm.

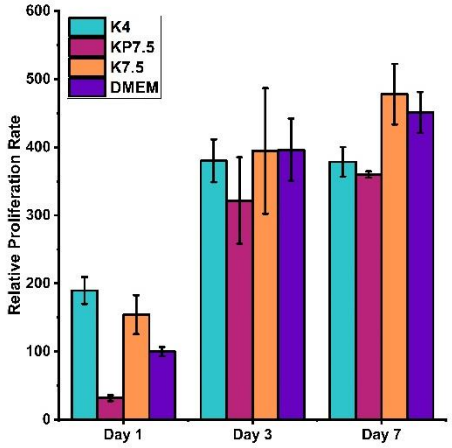

Figure 4.12. Cell proliferation results of K4, KP7.5 and K7.5 hydrogels.

Cell proliferation data for KTSMA and F127MA hydrogels were obtained by culturing 3T3 cells at a density of 2500 cells per well and are given in Figure 4.12. The cell density was determined fluorometrically using the Alamar Blue protocol. 3T3 cells cultured on TCPs were used as the control group. The hydrogels were conditioned in DMEM for one day before cell culturing. Fluorescence measurements were taken on the first, third, and seventh days after cell culturing and compared with the TCP data from the first day. Notably, the cell proliferation rate of F127MA hydrogel was initially lower than the other groups on the first day. However, it accelerated to the TCPs and KTSMA groups by the third day. In general, it was observed that KTSMA and F127MA hydrogels supported cell proliferation at rates very close to the control group.

4.2. Characterization of Curcumin and L-Lysine Carbon Dots

In the synthesis of carbon dots, lysine, and curcumin were selected as precursors. Curcumin extracted from Curcuma longa has antioxidant, anti-microbial, anticancer, and anti-inflammatory properties. However, poor water solubility limits its applications. The soluble form of the curcumin can be obtained in the carbon dot form by co-carbonizing it with soluble precursors such as urea and citric acid [85,86] In this study; lysine was used to enhance the solubility of curcumin-based carbon dots as well as its antibacterial, and cell attachment properties. Thus, we combined the properties of curcumin and lysine in a carbon dot platform to obtain antibacterial and antioxidant materials that will be useful in wound healing applications.

Thermal degradation behavior of curcumin and lysine, carbon dot raw materials, were observed using thermogravimetric analysis. TGA and DTGA curves are given in

Figure 4.13. Lysine presented three endotherms. The first endotherm at ~94ºC corresponds to the evaporation of volatiles, mainly water. The two endotherms at ~340ºC and ~570ºC indicate two-step thermal degradation. Similarly, curcumin exhibited two-step degradation. For both samples, the onset of degradation was observed below 300ºC. Thus, as a first attempt, curcumin and lysine were kept at 250ºC and observed to form carbon dots with high yield at this temperature and no other temperature was tested.

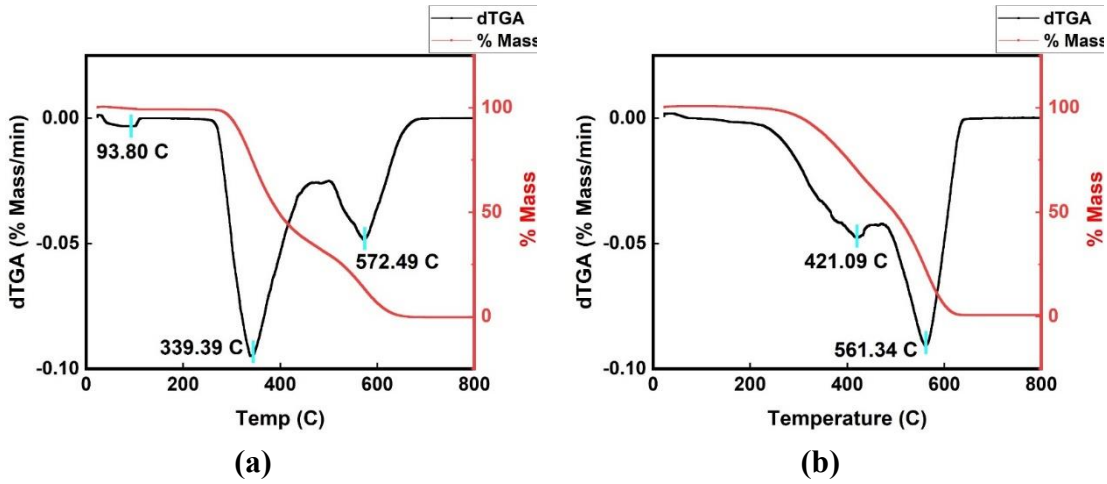

Figure 4.13. TGA curves of l-lysine (a) and curcumin (b).

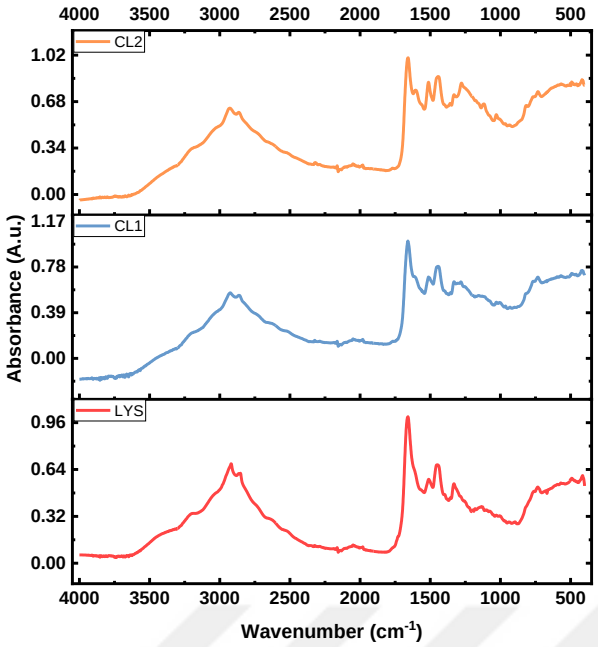

Figure 4.14. ATR-FTIR spectra of lysine, CL1 and CL2 CDs.

We synthesized three carbon dots composed of lysine only (LYS), lysine, and curcumin with a 1:5 and 1:2 curcumin: lysine ratio by weight denoted as CL1, and CL2, respectively. Functional groups of the CDs were determined with ATR-FTIR spectra given in Figure 4.14.

The ATR-FTIR spectra of CDs, and carbonyl groups were revealed at ~1659 and ~1512 cm^{-1}. The bands between 2800-3000 cm^{-1} bands correspond to alkanes, C-H stretching, whereas the band between 3000-3100 cm^{-1} indicates stretching of C-H group of alkenes, confirming the presence of the ring structure. A broad band at 3300 – 3500 can be due to -OH and -NH stretching vibrations. Thus, ATR spectra indicate the presence of -OH, -C=O, and -NH functional groups on the surface of the carbon dots.

XRD spectra of the CDs are given in Figure 4.15. All the spectra have a broad peak centered at 22.5° indicating 002 plane of graphitic structure.[76] A Sharp diffraction peak at 32° and small diffraction peaks between 40 and 60 degrees observed in CL2 suggest the unsymmetric arrangement of the carbon atoms.[87]

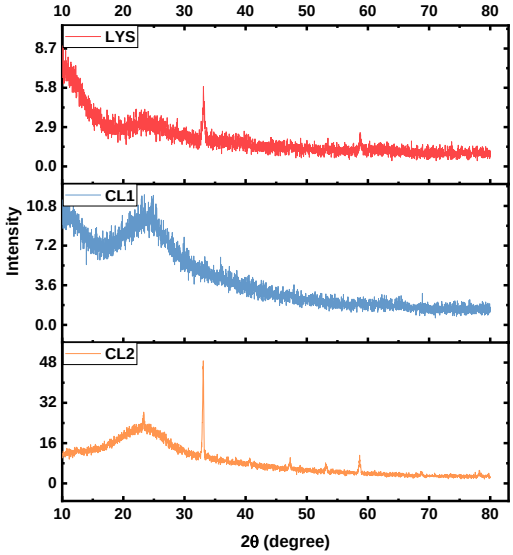

Figure 4.15. XRD data of lysine, CL1 and CL2 CDs.

Optical properties of the CDs were determined using UV-Vis and PL spectroscopy as given in Figure 4.16. In the UV-Vis spectra of the CDs, a weak absorption band observed between 275 and 300 nm corresponds to π-π* transition. PL spectra of both carbon dots exhibited a peak at ~420 nm corresponding to the blue region of the spectra suggesting their potential in bioimaging and sensing applications.

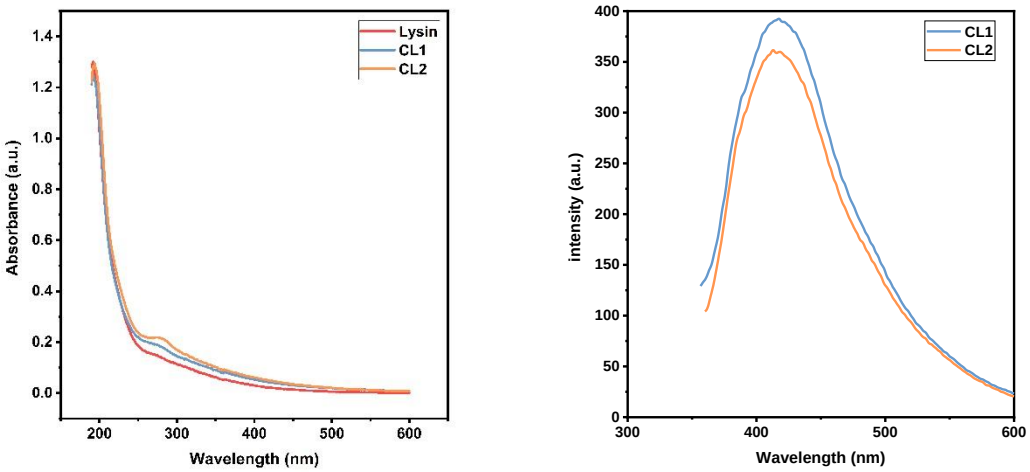

(a) **(b)**

Figure 4.16. UV-Vis (a) and PL (b) spectra of the CDs.

Particle size distributions of the CDs obtained by DLS are presented in Figure 4.16, D50 values of the LYS, CL1, and CL2 were determined as 69 nm, 4 nm, and 35 nm, respectively. In most studies, particle sizes of CDs are reported to be less than 10 nm. Thus, LYS and CL2 CDs have a more hydrophobic nature with high aggregation tendencies.

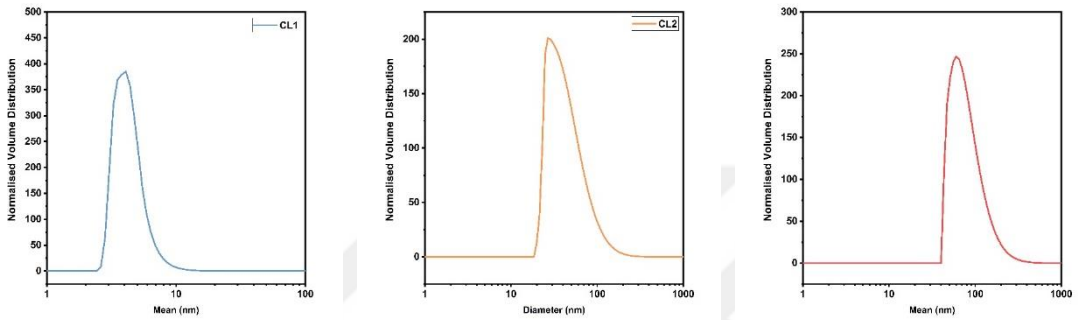

(a) **(b)** **(c)**

Figure 4.17. Particle size analysis of the CDs.

The antibacterial disc diffusion analysis images are given in Figure 4.18. The measurements were taken from 3 different sides of each Oxoid disc. The CDs showed an antibacterial effect against *S. aureus* with a zone diameter between 0.5 to 1 mm, but there were no effects against *E. coli*. This difference may be attributed to the fact that *E. coli* is classified as a gram-negative bacterium, whereas *S. aureus* is gram-positive. Gram-negative bacteria such as *E. coli* are generally more resistant to treatment due to the complexity and composition of their cell walls. This structural characteristic makes them more challenging to eliminate compared to gram-positive bacteria like *S. aureus*.[88]

The cell viability data obtained by culturing 3T3 cells at a density of 10,000 cells are shown in Figure 4.19. TCPs were used as the control group. According to these results, all three CDs show an acceptable cytotoxicity. For LYS and CL1, the highest viability was observed with the 0.5 mg/mL concentration and with increasing concentration, viability decreased slightly. For the CL2 cell viability was obtained as independently of its concentration.[76]

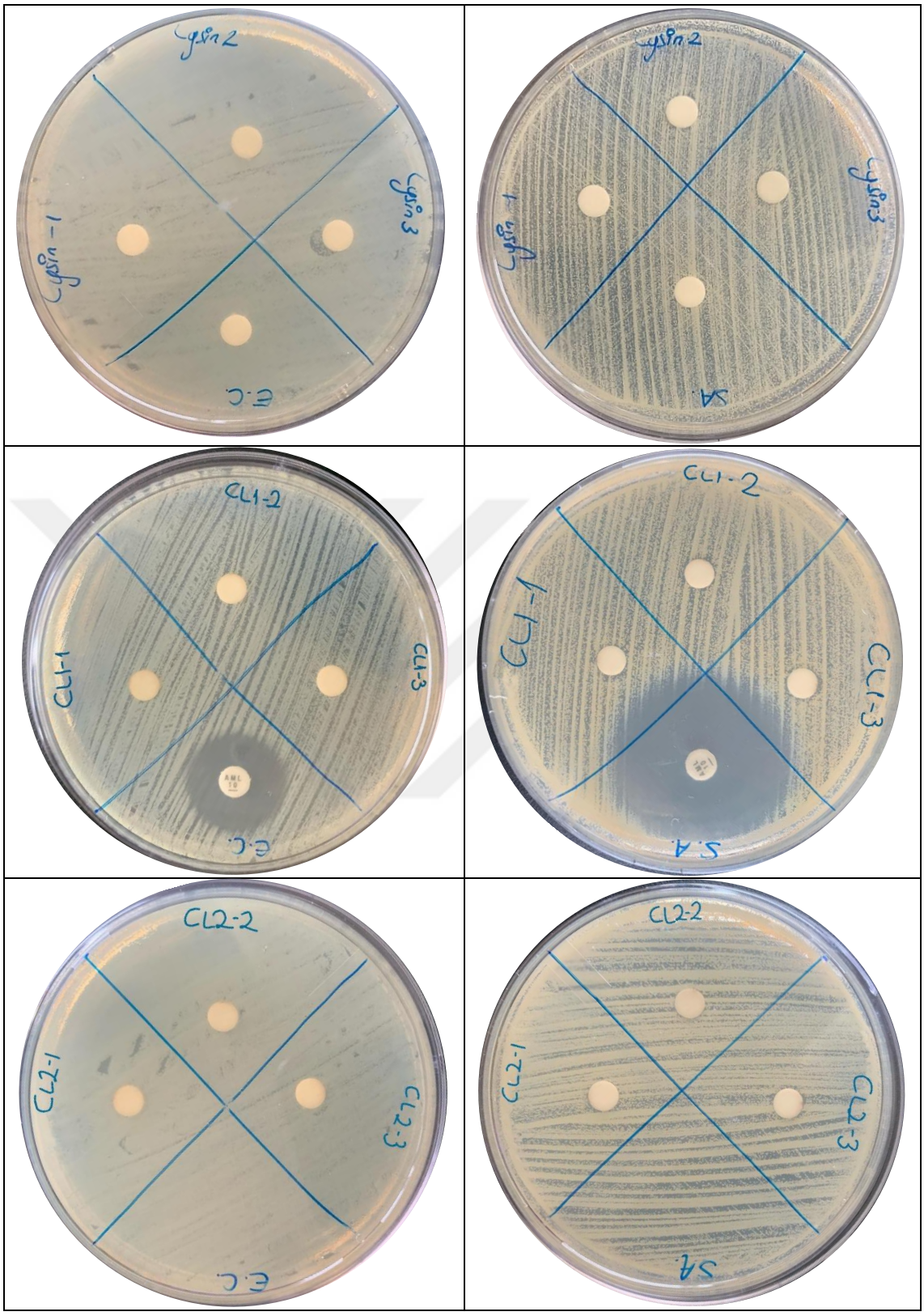

Figure 4.18. Antibacterial disc diffusion analysis of the CDs.

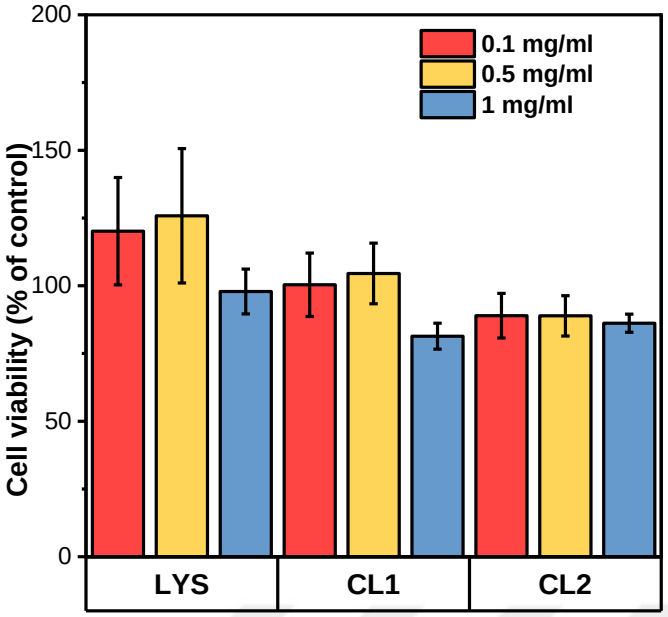

Figure 4.19. Cell viability of the CDs.

4.3. Characterization of Gallic Acid Loaded KTSMA Hydrogels

In the characterization of gallic acid-containing hydrogels, cytotoxicity was the initial step (Figure 4.20). The control medium, DMEM, was used for this test, and hydrogels containing 4 different concentrations of gallic acid were prepared. After suspending the hydrogels in the medium for 24h, the media containing hydrogel extracts were transferred to the plates where the cells had been previously seeded. Cell densities were assessed using the Alamar Blue Protocol. The hydrogels containing GA less than 0.5 mg/ml, exhibited acceptable cytotoxicity, and higher cytotoxicity was obtained as GA concentration increased, as expected.

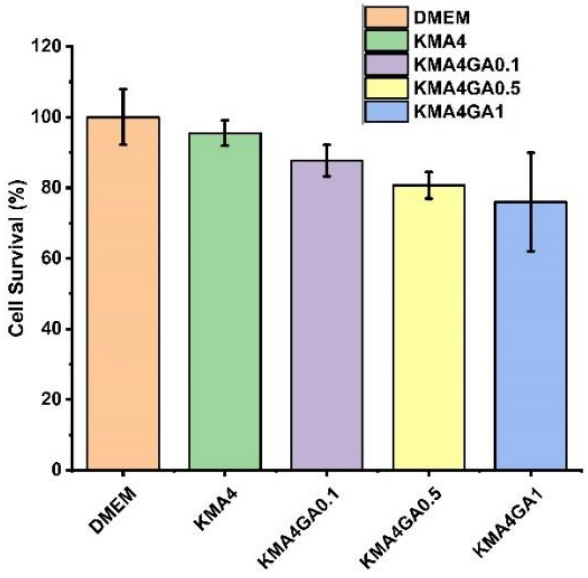

Figure 4.20. Cytotoxicity of GA loaded KTSMA hydrogels.

The antimicrobial testing results of the hydrogel extracts obtained using PBS are given in Figure 4.21. For the antibiotic, the zone diameter was measured as 6 mm against the complex cell wall of the gram-negative *E. coli* bacteria used. The zone widths of K4, K4GA0.1, K4GA0.5, and K4GA1 hydrogel extracts were obtained as 0, 0.05, 0.15, and 0.03 mm, respectively. For the gram-positive *S. aureus*, the zone diameter of the antibiotic disk was measured as 1.5 cm, and the zone widths cleared by the extracts of K4, K4GA0.1, K4GA0.5, and K4GA1 hydrogels were observed as 0, 0.25, 0.2, and 0.15 mm, respectively. Thus, the samples with gallic acid show modest antibacterial activity.

The antioxidant scavenging ratios were obtained using the DPPH method. The K4 hydrogel did not show any antioxidant activity whereas K4GA0.5 hydrogels exhibited an antioxidant scavenging ratio of 61.95±1.3%, confirming the antioxidant property of gallic acid.

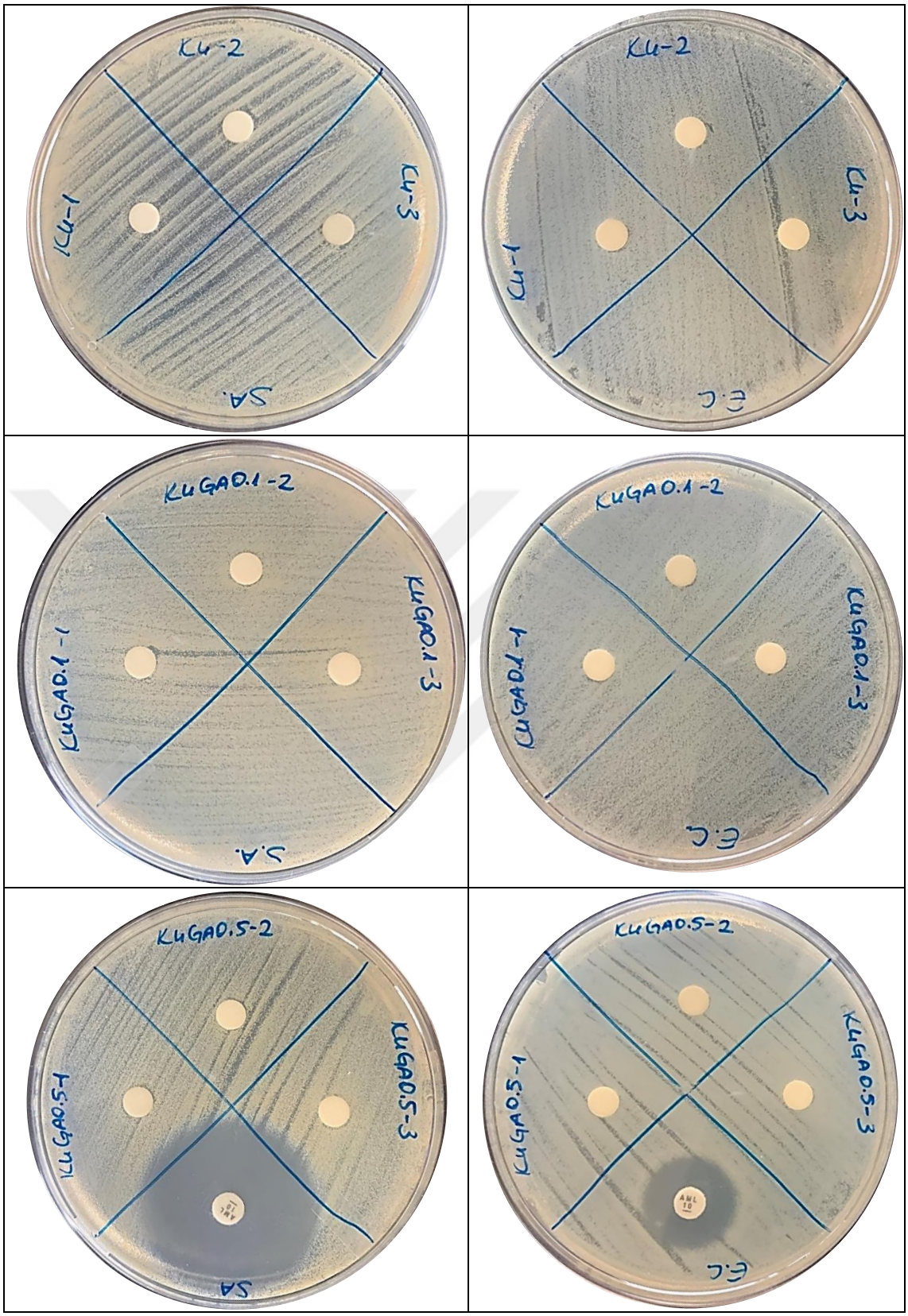

(cont. on next page)

Figure 4.21. Antimicrobial disc diffusion results of GA loaded hydrogels.

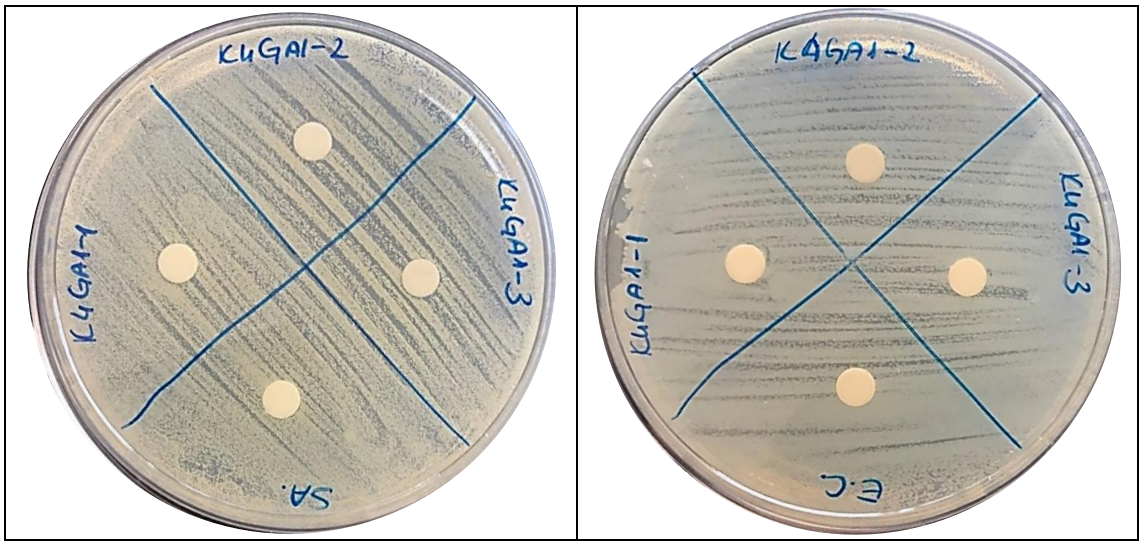

Figure 4.21 (cont.).

4.4. Characterization of GA and CD Loaded Hydrogels

For the final part of this study, GA and CDs loaded hydrogels were prepared. In section 4.3, GA-loaded hydrogels were prepared with K4 hydrogels due to their high viability and resistance to degradation. However, the mechanical properties of GA-loaded K4 hydrogels became inferior upon loading. Thus, GA and CDs were loaded to KP7.5 hydrogels due to the more robust mechanical properties and degradation resistance of pluronic-containing hydrogel, KP7.5. Viscoelastic properties, cytotoxicity, and antioxidant activity of the GA and CD-loaded KP7.5 hydrogels were determined. Preliminary wound healing potentials of these hydrogels were assessed using scratch test.

The frequency sweep and strain sweep results of the GA and CD-loaded hydrogels are given in Figure 4.22. For all samples, G’ values are consistently higher than G" values, confirming the three-dimensional network structure. Upon CD and/or GA loading, G' values of the hydrogels decreased noticeably. For KPGA, KPCD, and KPGACD hydrogels, G' values were obtained as 666 ± 218, 855 ± 211, and 385 ± 98 Pa, respectively, which could be attributed to the radical scavenging properties of GA and CD reducing the photocrosslinking efficiency. Strain sweep curves show the linear viscoelastic region (LVR). For all hydrogels, LVR corresponds to 10% strain.

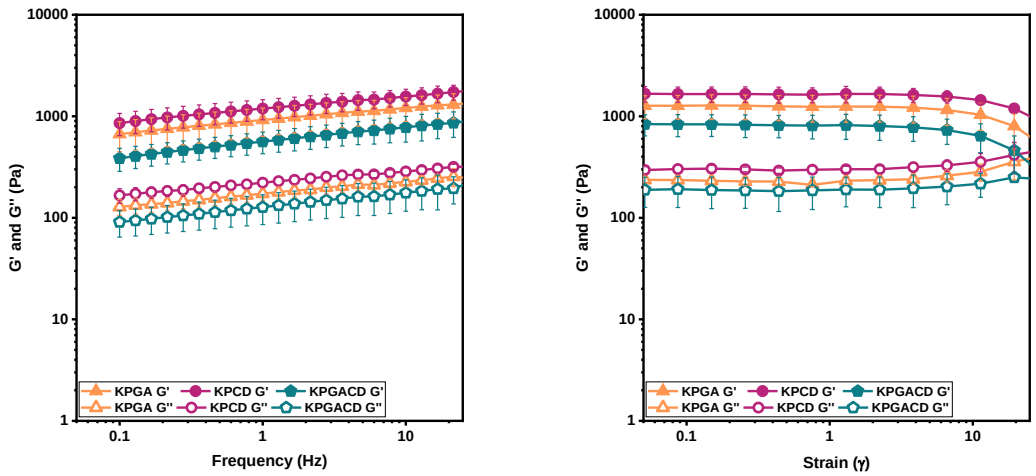

(a) **(b)**

Figure 4.22. Frequency (a) and strain (b) sweep data for KPGACD hydrogels.

Cytotoxicity data for the GA and CD-loaded KP7.5 hydrogels are given in Figure 4.23. All the hydrogel extracts indicated similar cell viability as DMEM confirming biocompatibility of the hydrogels.

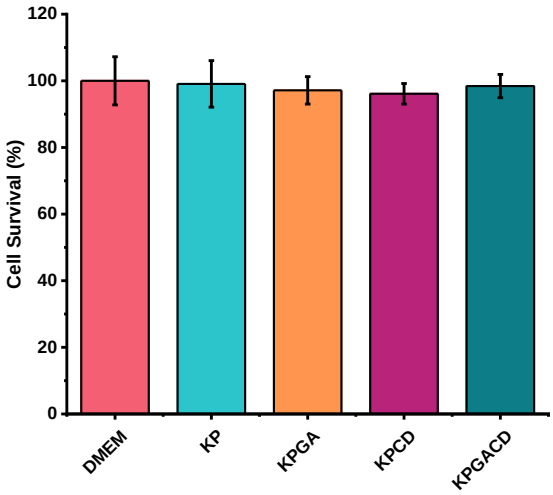

Figure 4.23. Cytotoxicity of GA-CD loaded hydrogels.

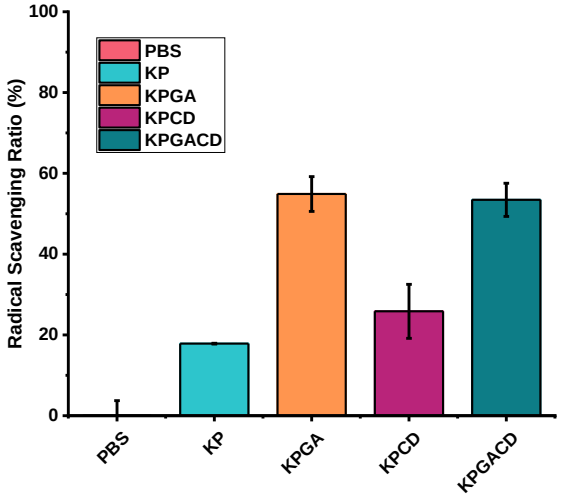

Figure 4.24. Antioxidant properties of GA-CD loaded hydrogels.

Free radical DPPH scavenging ratios were given in Figure 4.24. Unloaded and CD-loaded hydrogels exhibited slight antioxidant activity. However, both GA-loaded hydrogels presented scavenging ratios about 50-55% indicating that the antioxidant properties of the hydrogels are mainly governed by GA rather than CDs.

Scratch assay microscope images are shown in Figure 4.25. The wounds were closed at the end of 48h for all treatments. No significant differences between the samples were observed.

Sample Name	Before Scratch	The scratch	24 hours later	48 hours later
KP7.5	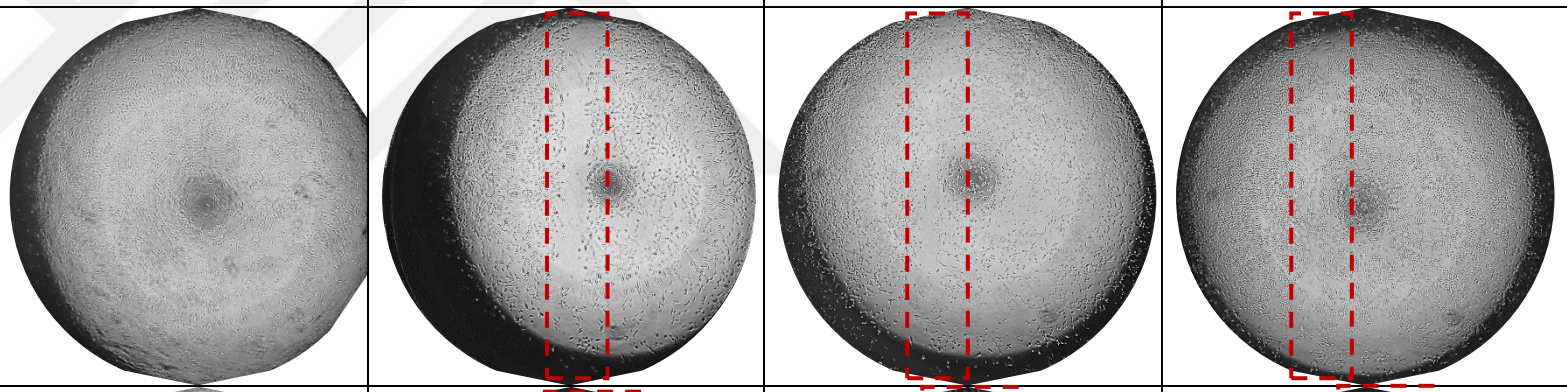			
KPGA				

(cont. on next page)

Figure 4.25. Scratch assay results of GA-CD loaded hydrogels.

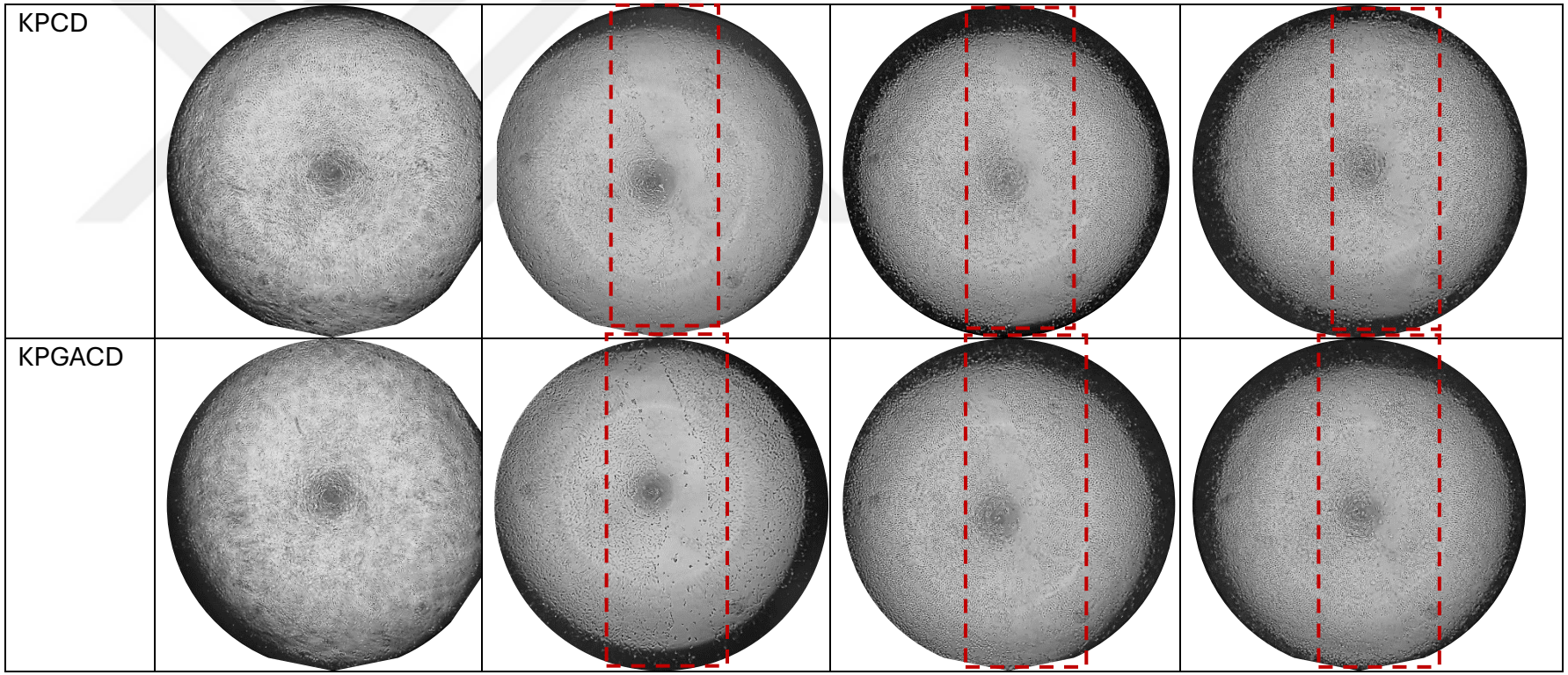

(cont. on next page)

Figure 4. 25 (cont.).

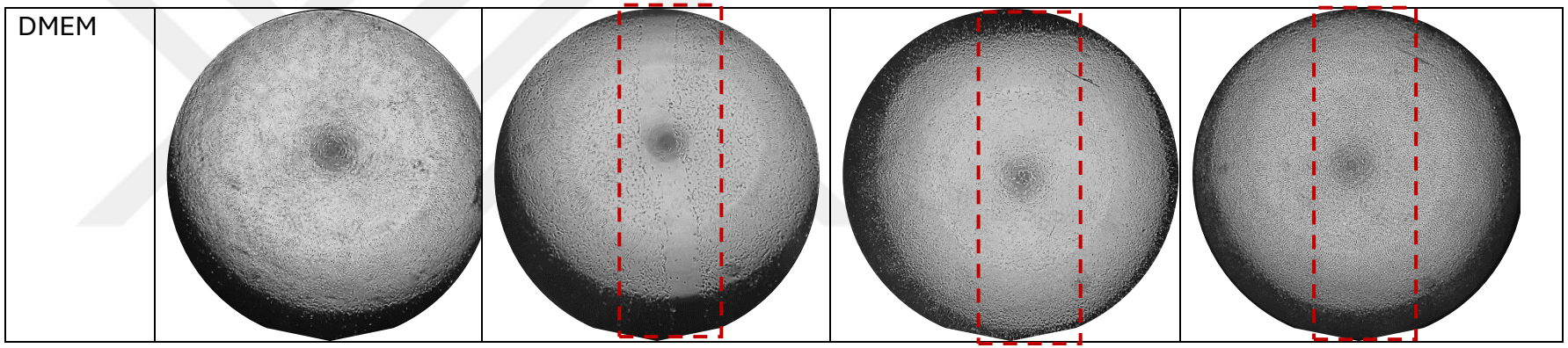

Figure 4. 25 (cont.).

CHAPTER 5

CONCLUSIONS AND FUTURE WORK

In the first part of this study, photocrosslinked hydrogels with varying compositions were prepared and characterized. Methacrylated forms of the keratose (oxidized keratin) and F127 were used in the hydrogel formulations. Increasing the concentration of keratose improved the mechanical properties of the hydrogels, whereas it accelerated the hydrolytic degradation. Using a synthetic polymer, F127, along with the keratose in the hydrogel formulations, on the other hand, improved their mechanical and degradation properties. Although initially, these hybrid hydrogels promoted cell growth slowly, after the third day, they presented similar cell proliferation rates as the keratose-only hydrogels.

In the second part, carbon dots were synthesized using curcumin and L-lysine, which have antibacterial and antioxidant properties beneficial for wound healing. These carbon dots exhibited peaks at the blue region of the fluorescence spectra, suggesting their potential in bioimaging and sensing applications. Additionally, they exhibited modest antibacterial activity against a gram-positive bacterium, S. aureus, and their antioxidant properties will be determined.

Finally, in the third part, multifunctional hydrogels containing gallic acid and carbon dots were prepared by photocrosslinking methacrylated forms of keratose and Pluronic F127. These hydrogels were shown to be biocompatible, and gallic acid-containing hydrogels especially presented notable antioxidant properties. Thus, they have a potential in wound healing applications. In future work, their antibacterial and hemocompatibility tests will be performed, and their cell attachment properties will be investigated.

REFERENCES

1. Kumar, M. S. A. The Skin. In *Techniques in Small Animal Wound Management*. Wiley March 29, 2024, pp 1–36. DOI: 10.1002/9781119933861.ch1.

2. Walters, K. A.; Roberts, M. S. The Structure and Function of Skin. In Drugs and the Pharmaceutical Sciences; CRC Press, 2002; pp 1–39.

3. Masri, S.; Zawani, M.; Zulkiflee, I.; Salleh, A.; Fadilah, N. I. M.; Maarof, M.; Wen, A. P. Y.; Duman, F.; Tabata, Y.; Aziz, I. A.; Idrus, R. B. H.; Fauzi, M. B. Cellular Interaction of Human Skin Cells towards Natural Bioink via 3d-Bioprinting Technologies for Chronic Wound: A Comprehensive Review. *Int J Mol Sci* **2022**, *23* (1). DOI: 10.3390/IJMS23010476.

4. Liu, P.; Zhu, J.-Y.; Tang, B.; Hu, Z.-C. Three-dimensional Digital Reconstruction of Skin Epidermis and Dermis. J. Microsc. **2018**, 270 (2), 170–175. DOI:10.1111/jmi.12671.

5. Ali, S.; Shabbir, M.; Shahid, N. The Structure of Skin and Transdermal Drug Delivery System-A Review. Res. J. Pharm. Technol. **2015**, 8 (2), 103. DOI:10.5958/0974-360x.2015.00019.0.

6. Kolarsick, P. A. J.; Kolarsick, M. A.; Goodwin, C. Anatomy and Physiology of the Skin. J. Dermatol. Nurses Assoc. **2011**, 3 (4), 203–213. DOI:10.1097/jdn.0b013e3182274a98.

7. Yadav, N.; Parveen, S.; Chakravarty, S.; Banerjee, M. Skin Anatomy and Morphology. In Skin Aging & Cancer; Springer Singapore: Singapore, **2019**; pp 1–10. DOI: 10.1007/978-981-13-2541-0_1

8. Sriram, G.; Bigliardi, P. L.; Bigliardi-Qi, M. Fibroblast Heterogeneity and Its Implications for Engineering Organotypic Skin Models in Vitro. Eur. J. Cell Biol. **2015**, 94 (11), 483–512. DOI: 10.1016/j.ejcb.2015.08.001.

9. Gilaberte, Y.; Prieto-Torres, L.; Pastushenko, I.; Juarranz, Á. Anatomy and Function of the Skin. In Nanoscience in Dermatology; Elsevier, **2016**; pp 1–14. DOI: 10.1016/B978-0-12-802926-8.00001-X.

10. Tottoli, E. M.; Dorati, R.; Genta, I.; Chiesa, E.; Pisani, S.; Conti, B. Skin Wound Healing Process and New Emerging Technologies for Skin Wound Care and Regeneration. Pharmaceutics **2020**, 12 (8), 735. DOI:10.3390/pharmaceutics12080735.

11. Gurtner, G. C.; Werner, S.; Barrandon, Y.; Longaker, M. T. Wound Repair and Regeneration. *Nature* **2008**, *453* (7193), 314–321. DOI: 10.1038/NATURE07039.

12. Singer, A. J.; Clark, R. A. F. Cutaneous Wound Healing. *New England Journal of Medicine* **1999**, *341* (10), 738–746. DOI: 10.1056/NEJM199909023411006.

13. Eming, S. A.; Martin, P.; Tomic-Canic, M. Wound Repair and Regeneration: Mechanisms, Signaling, and Translation. *Sci. Transl. Med.* **2014**, *6* (265). DOI:10.1126/scitranslmed.3009337.

14. Yang, G. H.; Lee, Y. B.; Kang, D.; Choi, E.; Nam, Y.; Lee, K. H.; You, H.-J.; Kang, H. J.; An, S. H.; Jeon, H. Overcome the Barriers of the Skin: Exosome Therapy. *Biomater. Res.* **2021**, *25* (1). DOI: 10.1186/s40824-021-00224-8.

15. Ellis, S.; Lin, E. J.; Tartar, D. Immunology of Wound Healing. *Curr. Dermatol. Rep.* **2018**, *7* (4), 350–358. DOI:10.1007/s13671-018-0234-9.

16. Selvaraj, D.; Viswanadha Vijaya, P.; Elango, S. Wound Dressings – a Review. *BioMedicine (Taipei)* **2015**, *5* (4). DOI: 10.7603/s40681-015-0022-9.

17. Farahani, M.; Shafiee, A. Wound Healing: From Passive to Smart Dressings. *Adv. Healthc. Mater.* **2021**, *10* (16). DOI: 10.1002/adhm.202100477.

18. Rezvani Ghomi, E.; Niazi, M.; Ramakrishna, S. The Evolution of Wound Dressings: From Traditional to Smart Dressings. *Polym. Adv. Technol.* **2023**, *34* (2), 520–530. DOI:10.1002/pat.5929.

19. Rezvani Ghomi, E.; Khalili, S.; Nouri Khorasani, S.; Esmaeely Neisiany, R.; Ramakrishna, S. Wound Dressings: Current Advances and Future Directions. *J. Appl. Polym. Sci.* **2019**, *136* (27). DOI:10.1002/app.47738.

20. Zoellner, P.; Kapp, H.; Smola, H. Clinical Performance of a Hydrogel Dressing in Chronic Wounds: A Prospective Observational Study. *J. Wound Care* **2007**, *16* (3), 133–136. DOI: 10.12968/jowc.2007.16.3.27019.

21. Boateng, J. S.; Matthews, K. H.; Stevens, H. N. E.; Eccleston, G. M. Wound Healing Dressings and Drug Delivery Systems: A Review. *J. Pharm. Sci.* **2008**, *97* (8), 2892–2923. DOI: 10.1002/jps.21210.

22. Kus, K. J. B.; Ruiz, E. S. Wound Dressings – A Practical Review. *Curr. Dermatol. Rep.* **2020**, *9* (4), 298–308. DOI: 10.1007/s13671-020-00319-w.

23. Broussard, K. C.; Powers, J. G. Wound Dressings: Selecting the Most Appropriate Type. *Am. J. Clin. Dermatol.* **2013**, *14* (6), 449–459. DOI: 10.1007/s40257-013-0046-4.

24. Ghomi, E. R.; Lakshminarayanan, R.; Chellappan, V.; Verma, N. K.; Chinnappan, A.; Neisiany, R. E.; Amuthavalli, K.; Poh, Z. S.; Wong, B. H. S.; Dubey, N.; Narayan, R.; Ramakrishna, S. Electrospun Aligned PCL/Gelatin Scaffolds Mimicking the Skin ECM for Effective Antimicrobial Wound Dressings. *Adv. Fiber Mater.* **2023**, *5* (1), 235–251. DOI: 10.1007/s42765-022-00216-w.

25. Ribeiro, M. P.; Espiga, A.; Silva, D.; Baptista, P.; Henriques, J.; Ferreira, C.; Silva, J. C.; Borges, J. P.; Pires, E.; Chaves, P.; Correia, I. J. Development of a New Chitosan Hydrogel for Wound Dressing. *Wound Repair Regen.* **2009**, *17* (6), 817–824. DOI: 10.1111/j.1524-475x.2009.00538.x.

26. Wichterle, O.; Lím, D. Hydrophilic Gels for Biological Use. *Nature* **1960**, *185* (4706), 117–118. DOI: 10.1038/185117a0.

27. Gyles, D. A.; Castro, L. D.; Silva, J. O. C., Jr; Ribeiro-Costa, R. M. A Review of the Designs and Prominent Biomedical Advances of Natural and Synthetic Hydrogel Formulations. *Eur. Polym. J.* **2017**, *88*, 373–392. DOI:10.1016/j.eurpolymj.2017.01.027.

28. Ahmed, E. M. Hydrogel: Preparation, Characterization, and Applications: A Review. *J. Adv. Res.* **2015**, *6* (2), 105–121. DOI: 10.1016/j.jare.2013.07.006.

29. Hennink, W. E.; van Nostrum, C. F. Novel Crosslinking Methods to Design Hydrogels. *Adv. Drug Deliv. Rev.* **2012**, *64*, 223–236. DOI: 10.1016/j.addr.2012.09.009.

30. Hu, W.; Wang, Z.; Xiao, Y.; Zhang, S.; Wang, J. Advances in Crosslinking Strategies of Biomedical Hydrogels. *Biomater. Sci.* **2019**, *7* (3), 843–855. DOI:10.1039/c8bm01246f.

31. Parhi, R. Cross-Linked Hydrogel for Pharmaceutical Applications: A Review. *Adv. Pharm. Bull.* **2017**, *7* (4), 515–530. DOI: 10.15171/apb.2017.064.

32. Liu, J.; Su, C.; Chen, Y.; Tian, S.; Lu, C.; Huang, W.; Lv, Q. Current Understanding of the Applications of Photocrosslinked Hydrogels in Biomedical Engineering. *Gels* **2022**, *8* (4), 216. DOI: 10.3390/gels8040216.

33. Liang, J.; Dijkstra, P. J.; Poot, A. A.; Grijpma, D. W. Hybrid Hydrogels Based on Methacrylate-Functionalized Gelatin (GelMA) and Synthetic Polymers. *Biomed. Mater. Devices* **2023**, *1* (1), 191–201. DOI:10.1007/s44174-022-00023-2.

34. Oliveira, C.; Sousa, D.; Teixeira, J. A.; Ferreira-Santos, P.; Botelho, C. M. Polymeric Biomaterials for Wound Healing. *Front. Bioeng. Biotechnol.* **2023**, *11*. DOI:10.3389/fbioe.2023.1136077.

35. Zhong, S. P.; Zhang, Y. Z.; Lim, C. T. Tissue Scaffolds for Skin Wound Healing and Dermal Reconstruction. *Wiley Interdiscip. Rev. Nanomed. Nanobiotechnol.* **2010**, *2* (5), 510–525. DOI:10.1002/wnan.100.

36. Negut, I.; Dorcioman, G.; Grumezescu, V. Scaffolds for Wound Healing Applications. *Polymers (Basel)* **2020**, *12* (9), 2010. DOI:10.3390/polym12092010.

37. Gioffredi, E.; Boffito, M.; Calzone, S.; Giannitelli, S. M.; Rainer, A.; Trombetta, M.; Mozetic, P.; Chiono, V. Pluronic F127 Hydrogel Characterization and

Biofabrication in Cellularized Constructs for Tissue Engineering Applications. *Procedia CIRP* **2016**, *49*, 125–132. DOI: 10.1016/j.procir.2015.11.001.

38. Dantas Silva, L. A. S.; da Cruz de Jesus, R. L.; Fiuza-Junior, R. A.; Andrade, H. M. C.; Rigoli, I. C.; de Assunção, R. M. N.; Barichello, J. M.; de Lima, R. G. Aloe Vera Gel Influence on the Micellization Behavior of Copolymer Pluronic F127: A Potential Photosensitizer Carrier for Topical Application. *J. Appl. Polym. Sci.* **2018**, *135* (17). DOI:10.1002/app.46191.

39. Diniz, I. M. A.; Chen, C.; Xu, X.; Ansari, S.; Zadeh, H. H.; Marques, M. M.; Shi, S.; Moshaverinia, A. Pluronic F-127 Hydrogel as a Promising Scaffold for Encapsulation of Dental-Derived Mesenchymal Stem Cells. *J. Mater. Sci. Mater. Med.* **2015**, *26* (3). DOI:10.1007/s10856-015-5493-4.

40. Li, S.; Yang, C.; Li, J.; Zhang, C.; Zhu, L.; Song, Y.; Guo, Y.; Wang, R.; Gan, D.; Shi, J.; Ma, P.; Gao, F.; Su, H. Progress in Pluronic F127 Derivatives for Application in Wound Healing and Repair. *Int. J. Nanomedicine* **2023**, *18*, 4485–4505. DOI: 10.2147/ijn.s418534.

41. Mukherjee, S.; Krishnan, A.; Athira, R. K.; Kasoju, N.; Sah, M. K. Silk Fibroin and Silk Sericin in Skin Tissue Engineering and Wound Healing: Retrospect and Prospects. In *Natural Polymers in Wound Healing and Repair*; Elsevier, 2022; pp 301–331. DOI: 10.1016/B978-0-323-90514-5.00005-5.

42. ter Horst, B.; Moiemen, N. S.; Grover, L. M. Natural Polymers: Biomaterials for Skin Scaffolds. *Biomaterials for Skin Repair and Regeneration* **2019**, 151–192. DOI: 10.1016/B978-0-08-102546-8.00006-6.

43. Shah, S. A.; Sohail, M.; Khan, S.; Minhas, M. U.; de Matas, M.; Sikstone, V.; Hussain, Z.; Abbasi, M.; Kousar, M. Biopolymer-Based Biomaterials for Accelerated Diabetic Wound Healing: A Critical Review. *Int. J. Biol. Macromol.* **2019**, *139*, 975–993. DOI: 10.1016/j.ijbiomac.2019.08.007.

44. Sando, L.; Kim, M.; Colgrave, M. L.; Ramshaw, J. A. M.; Werkmeister, J. A.; Elvin, C. M. Photochemical Crosslinking of Soluble Wool Keratins Produces a Mechanically Stable Biomaterial That Supports Cell Adhesion and Proliferation. *J. Biomed. Mater. Res. A* **2010**, *95A* (3), 901–911. DOI: 10.1002/jbm.a.32913.

45. Giteru, S. G.; Ramsey, D. H.; Hou, Y.; Cong, L.; Mohan, A.; Bekhit, A. E.-D. A. Wool Keratin as a Novel Alternative Protein: A Comprehensive Review of Extraction, Purification, Nutrition, Safety, and Food Applications. *Compr. Rev. Food Sci. Food Saf.* **2023**, *22* (1), 643–687. DOI: 10.1111/1541-4337.13087.

46. Patil, A. B.; Meng, Z.; Wu, R.; Ma, L.; Xu, Z.; Shi, C.; Qiu, W.; Liu, Q.; Zhang, Y.; Lin, Y.; Lin, N.; Liu, X. Y. Tailoring the Meso-Structure of Gold Nanoparticles in Keratin-Based Activated Carbon toward High-Performance Flexible Sensor. *Nanomicro Lett.* **2020**, *12* (1). DOI: 10.1007/s40820-020-00459-5.

47. Liang, Y.; He, J.; Guo, B. Functional Hydrogels as Wound Dressing to Enhance Wound Healing. *ACS Nano* **2021**, *15* (8), 12687–12722. DOI: 10.1021/acsnano.1c04206.

48. Jangde, R.; Srivastava, S.; Singh, M. R.; Singh, D. In Vitro and In Vivo Characterization of Quercetin Loaded Multiphase Hydrogel for Wound Healing Application. *Int. J. Biol. Macromol.* **2018**, *115*, 1211–1217. DOI: 10.1016/j.ijbiomac.2018.05.010.

49. Yang, D.; Chen, H.; Wei, H.; Liu, A.; Wei, D.-X.; Chen, J. Hydrogel Wound Dressings Containing Bioactive Compounds Originated from Traditional Chinese Herbs: A Review. *Smart Mater. Med.* **2024**, *5* (1), 153–165. DOI: 10.1016/j.smaim.2023.10.004.

50. Tajik, F.; Eslahi, N.; Rashidi, A.; Rad, M. M. Hybrid Antibacterial Hydrogels Based on PVP and Keratin Incorporated with Lavender Extract. *J. Polym. Res.* **2021**, *28* (8). DOI: 10.1007/s10965-021-02681-0.

51. Chen, G.; Yu, Y.; Wu, X.; Wang, G.; Ren, J.; Zhao, Y. Bioinspired Multifunctional Hybrid Hydrogel Promotes Wound Healing. *Adv. Funct. Mater.* **2018**, *28* (33). DOI: 10.1002/adfm.201801386.

52. Zubik, K.; Singhsa, P.; Wang, Y.; Manuspiya, H.; Narain, R. Thermo-Responsive Poly(N-Isopropylacrylamide)-Cellulose Nanocrystals Hybrid Hydrogels for Wound Dressing. *Polymers (Basel)* **2017**, *9* (4), 119. DOI:10.3390/polym9040119.

53. Masood, N.; Ahmed, R.; Tariq, M.; Ahmed, Z.; Masoud, M. S.; Ali, I.; Asghar, R.; Andleeb, A.; Hasan, A. Silver Nanoparticle Impregnated Chitosan-PEG Hydrogel Enhances Wound Healing in Diabetes Induced Rabbits. *Int. J. Pharm.* **2019**, *559*, 23–36. DOI: 10.1016/j.ijpharm.2019.01.019.

54. Gupta, A.; Briffa, S. M.; Swingler, S.; Gibson, H.; Kannappan, V.; Adamus, G.; Kowalczuk, M.; Martin, C.; Radecka, I. Synthesis of Silver Nanoparticles Using Curcumin-Cyclodextrins Loaded into Bacterial Cellulose-Based Hydrogels for Wound Dressing Applications. *Biomacromolecules* **2020**, *21* (5), 1802–1811. DOI: 10.1021/acs.biomac.9b01724.

55. Maitra, J.; Shukla, V. K.; Kumar Shukla, V. Cross-Linking in Hydrogels-a Review. *American Journal of Polymer Science* **2014**, *2014* (2), 25–31. DOI: 10.5923/j.ajps.20140402.01.

56. Kahkeshani, N.; Farzaei, F.; Fotouhi, M.; Alavi, S. S.; Bahramsoltani, R.; Naseri, R.; Momtaz, S.; Abbasabadi, Z.; Rahimi, R.; Farzaei, M. H.; Bishayee, A. Pharmacological Effects of Gallic Acid in Health and Diseases: A Mechanistic Review. *Iran J. Basic Med. Sci.* **2019**, *22* (3), 225. DOI:10.22038/ijbms.2019.32806.7897.

57. Gan, J.-E.; Chin, C.-Y. Formulation and Characterisation of Alginate Hydrocolloid Film Dressing Loaded with Gallic Acid for Potential Chronic Wound Healing. *F1000Res.* **2021**, *10*, 451. DOI:10.12688/f1000research.52528.1.

58. Zong, Q.; Chen, H.; Zhao, Y.; Wang, J.; Wu, J. Bioactive Carbon Dots for Tissue Engineering Applications. *Smart Mater. Med.* **2024**, *5* (1), 1–14. DOI: 10.1016/j.smaim.2023.06.006.

59. Xu, X.; Ray, R.; Gu, Y.; Ploehn, H. J.; Gearheart, L.; Raker, K.; Scrivens, W. A. Electrophoretic Analysis and Purification of Fluorescent Single-Walled Carbon Nanotube Fragments. *J. Am. Chem. Soc.* **2004**, *126* (40), 12736–12737. DOI:10.1021/ja040082h.

60. Ghirardello, M.; Ramos-Soriano, J.; Galan, M. C. Carbon Dots as an Emergent Class of Antimicrobial Agents. *Nanomaterials (Basel)* **2021**, *11* (8), 1877. DOI:10.3390/nano11081877.

61. Jakubczyk, K.; Drużga, A.; Katarzyna, J.; Skonieczna-Żydecka, K. Antioxidant Potential of Curcumin—A Meta-Analysis of Randomized Clinical Trials. *Antioxidants (Basel)* **2020**, *9* (11), 1092. DOI:10.3390/antiox9111092.

62. Schaffer, M.; Schaffer, P. M.; Bar-Sela, G. An Update on Curcuma as a Functional Food in the Control of Cancer and Inflammation. *Curr. Opin. Clin. Nutr. Metab. Care* **2015**, *18* (6), 605–611. DOI: 10.1097/mco.0000000000000227.

63. Zheng, D.; Huang, C.; Huang, H.; Zhao, Y.; Khan, M. R. U.; Zhao, H.; Huang, L. Antibacterial Mechanism of Curcumin: A Review. *Chem. Biodivers.* **2020**, *17* (8). DOI: 10.1002/cbdv.202000171.

64. Wu, L.; Gao, Y.; Zhao, C.; Huang, D.; Chen, W.; Lin, X.; Liu, A.; Lin, L. Synthesis of Curcumin-Quaternized Carbon Quantum Dots with Enhanced Broad-Spectrum Antibacterial Activity for Promoting Infected Wound Healing. *Biomater. Adv.* **2022**, *133* (112608), 112608. DOI: 10.1016/j.msec.2021.112608.

65. Leong, C. R.; Tong, W. Y.; Tan, W.-N.; Tumin, N. D.; Yusof, F. A. M.; Yacob, L. S.; Rosli, M. I. H. B.; Md Abu, T. Synthesis of Curcumin Quantum Dots and Their Antimicrobial Activity on Necrotizing Fasciitis Causing Bacteria. *Mater. Today* **2020**, *31*, 31–35. DOI: 10.1016/j.matpr.2020.01.082.

66. Shashikumara, S.; Jayaraman, V.; Chikkegowda, P.; Lingaiah, D. C.; Kalal, B. S. Efficacy of 15% Lysine Cream in Treating Diabetic Foot Ulcers: A Randomized Interventional Study. *Int J Physiol Pathophysiol Pharmacol* **2023**, *15* (3), 88.

67. Betts, M. J.; Russell, R. B. Amino Acid Properties and Consequences of Substitutions. *Bioinformatics for Geneticists*. Wiley February 21, 2003, pp 289–316. DOI: 10.1002/0470867302.ch14.

68. Cao, Y.; Hu, G.; Li, W.; Wang, J.; Ge, Y.; Li, F.; Guo, W.; Kan, X.; Fu, S.; Liu, J. Lysine Promotes Proliferation and β-Casein Synthesis through the SLC6A14-

ERK1/2-CDK1-mTOR Signaling Pathway in Bovine Primary Mammary Epithelial Cells. *J. Therm. Biol.* **2022**, *110* (103375), 103375. DOI: 10.1016/j.jtherbio.2022.103375.

69. Lazzaro, B. P.; Zasloff, M.; Rolff, J. Antimicrobial Peptides: Application Informed by Evolution. *Science* **2020**, *368* (6490). DOI: 10.1126/science.aau5480.

70. Huan, Y.; Kong, Q.; Mou, H.; Yi, H. Antimicrobial Peptides: Classification, Design, Application and Research Progress in Multiple Fields. *Front. Microbiol.* **2020**, *11*. DOI: 10.3389/fmicb.2020.582779.

71. Wang, J.; Hao, S.; Luo, T.; Cheng, Z.; Li, W.; Gao, F.; Guo, T.; Gong, Y.; Wang, B. Feather Keratin Hydrogel for Wound Repair: Preparation, Healing Effect and Biocompatibility Evaluation. *Colloids Surf. B Biointerfaces* **2017**, *149*, 341–350. DOI: 10.1016/j.colsurfb.2016.10.038.

72. Stubbe, B.; Mignon, A.; Van Damme, L.; Claes, K.; Hoeksema, H.; Monstrey, S.; Van Vlierberghe, S.; Dubruel, P. Photo-crosslinked Gelatin-based Hydrogel Films to Support Wound Healing. *Macromol. Biosci.* **2021**, *21* (12). DOI: 10.1002/mabi.202100246.

73. Klotz, B. J.; Gawlitta, D.; Rosenberg, A. J. W. P.; Malda, J.; Melchels, F. P. W. Gelatin-Methacryloyl Hydrogels: Towards Biofabrication-Based Tissue Repair. *Trends Biotechnol.* **2016**, *34* (5), 394–407. DOI: 10.1016/j.tibtech.2016.01.002.

74. Sharun, K.; Banu, S. A.; Mamachan, M.; Subash, A.; Karikalan, M.; Vinodhkumar, O. R.; Manjusha, K. M.; Kumar, R.; Telang, A. G.; Dhama, K.; Pawde, A. M.; Maiti, S. K.; Amarpal. Pluronic F127 Composite Hydrogel for the Repair of Contraction Suppressed Full-Thickness Skin Wounds in a Rabbit Model. *Curr. Res. Transl. Med.* **2024**, *72* (4), 103458. DOI: 10.1016/j.retram.2024.103458.

75. Riaz, Z.; Baddi, S.; Gao, F.; Feng, C.-L. Gallic Acid-Doped Multifunctional Hybrid Hydrogel for Antioxidant and Antibacterial Studies. *Eur. Polym. J.* **2024**, *206* (112778), 112778. DOI: 10.1016/j.eurpolymj.2024.112778.

76. Li, P.; Han, F.; Cao, W.; Zhang, G.; Li, J.; Zhou, J.; Gong, X.; Turnbull, G.; Shu, W.; Xia, L.; Fang, B.; Xing, X.; Li, B. Carbon Quantum Dots Derived from Lysine and Arginine Simultaneously Scavenge Bacteria and Promote Tissue Repair. *Appl. Mater. Today* **2020**, *19* (100601), 100601. DOI: 10.1016/j.apmt.2020.100601.

77. Yalçın, D.; Top, A. Novel Biopolymer-Based Hydrogels Obtained through Crosslinking of Keratose Proteins Using Tetrakis(Hydroxymethyl) Phosphonium Chloride. *Iran. Polym. J.* **2022**, *31* (9), 1057–1067. DOI: 10.1007/s13726-022-01058-4.

78. Pakkaner, E.; Yalçın, D.; Uysal, B.; Top, A. Self-Assembly Behavior of the Keratose Proteins Extracted from Oxidized Ovis Aries Wool Fibers. *Int. J. Biol. Macromol.* **2019**, *125*, 1008–1015. DOI: 10.1016/j.ijbiomac.2018.12.129.

79. Lin-Gibson, S.; Bencherif, S.; Cooper, J. A.; Wetzel, S. J.; Antonucci, J. M.; Vogel, B. M.; Horkay, F.; Washburn, N. R. Synthesis and Characterization of PEG Dimethacrylates and Their Hydrogels. *Biomacromolecules* **2004**, *5* (4), 1280–1287. DOI: 10.1021/bm0498777.

80. Snyder, S. L.; Sobocinski, P. Z. An Improved 2,4,6-Trinitrobenzenesulfonic Acid Method for the Determination of Amines. *Anal. Biochem.* **1975**, *64* (1), 284–288. DOI: 10.1016/0003-2697(75)90431-5.

81. Galler, K. M.; Aulisa, L.; Regan, K. R.; D'Souza, R. N.; Hartgerink, J. D. Self-Assembling Multidomain Peptide Hydrogels: Designed Susceptibility to Enzymatic Cleavage Allows Enhanced Cell Migration and Spreading. *J. Am. Chem. Soc.* **2010**, *132* (9), 3217–3223. DOI: 10.1021/ja910481t.

82. Li, Z.; Yuan, B.; Dong, X.; Duan, L.; Tian, H.; He, C.; Chen, X. Injectable Polysaccharide Hybrid Hydrogels as Scaffolds for Burn Wound Healing. *RSC Adv.* **2015**, *5* (114), 94248–94256. DOI: 10.1039/c5ra16912g.

83. He, Y.; Liu, K.; Guo, S.; Chang, R.; Zhang, C.; Guan, F.; Yao, M. Multifunctional Hydrogel with Reactive Oxygen Species Scavenging and Photothermal Antibacterial Activity Accelerates Infected Diabetic Wound Healing. *Acta Biomater.* **2023**, *155*, 199–217. DOI: 10.1016/j.actbio.2022.11.023.

84. Liang, C.-C.; Park, A. Y.; Guan, J.-L. In Vitro Scratch Assay: A Convenient and Inexpensive Method for Analysis of Cell Migration in Vitro. *Nat. Protoc.* **2007**, *2* (2), 329–333. DOI: 10.1038/nprot.2007.30.

85. Pal, T.; Mohiyuddin, S.; Packirisamy, G. Facile and Green Synthesis of Multicolor Fluorescence Carbon Dots from Curcumin: *In Vitro* and *in Vivo* Bioimaging and Other Applications. *ACS Omega* **2018**, *3* (1), 831–843. DOI: 10.1021/acsomega.7b01323.

86. Fibriani, A.; Taharuddin, A. A. P.; Stephanie, R.; Yamahoki, N.; Laurelia, J.; Wisnuwardhani, P. H.; Agustiyanti, D. F.; Angelina, M.; Rubiyana, Y.; Ningrum, R. A.; Wardiana, A.; Iskandar, F.; Permatasari, F. A.; Giri-Rachman, E. A. Curcumin-Derived Carbon-Dots as a Potential COVID-19 Antiviral Drug. *Heliyon* **2023**, *9* (9), e20089. DOI: /10.1016/j.heliyon.2023.e20089.

87. Thulasi, S.; Kathiravan, A.; Asha Jhonsi, M. Fluorescent Carbon Dots Derived from Vehicle Exhaust Soot and Sensing of Tartrazine in Soft Drinks. *ACS Omega* **2020**, *5* (12), 7025–7031. DOI: 10.1021/acsomega.0c00707.

88. Sperandio, F.; Huang, Y.-Y.; Hamblin, M. Antimicrobial Photodynamic Therapy to Kill Gram-Negative Bacteria. *Recent Pat. Antiinfect. Drug Discov.* **2013**, *8* (2), 108–120. DOI: 10.2174/1574891x113089990012.